

Review

Carbon Capture from CO₂-Rich Natural Gas via Gas-Liquid Membrane Contactors with Aqueous-Amine Solvents: A Review

Guilherme Pereira da Cunha , José Luiz de Medeiros * and Ofélia de Queiroz F. Araújo 

Escola de Química, Federal University of Rio de Janeiro, CT, E, Ilha do Fundão, Rio de Janeiro 21941-909, RJ, Brazil
* Correspondence: jlm@eq.ufrj.br

Abstract: Gas–liquid membrane contactor is a promising process intensification technology for off-shore natural gas conditioning in which weight and footprint constraints impose severe limitations. Thanks to its potential for substituting conventional packed/trayed columns for acid-gas absorption and acid-gas solvent regeneration, gas-liquid membrane contactors have been investigated experimentally and theoretically in the past two decades, wherein aqueous-amine solvents and their blends are the most employed solvents for carbon dioxide removal from natural gas in gas-liquid membrane contactors. These efforts are extensively and critically reviewed in the present work. Experimentally, there are a remarkable lack of literature data in the context of gas–liquid membrane contactors regarding the following topics: water mass transfer; outlet stream temperatures; head-loss; and light hydrocarbons (e.g., ethane, propane, and heavier) mass transfer. Theoretically, there is a lack of complete models to predict gas-liquid membrane contactor operation, considering multicomponent mass balances, energy balances, and momentum balances, with an adequate thermodynamic framework for correct reactive vapor–liquid equilibrium calculation and thermodynamic and transport property prediction. Among the few works covering modeling of gas-liquid membrane contactors and implementation in professional process simulators, none of them implemented all the above aspects in a completely successful way.

Keywords: gas–liquid membrane contactor; natural gas conditioning; carbon capture; solvent regeneration; process intensification; process simulation



Citation: da Cunha, G.P.; de Medeiros, J.L.; Araújo, O.d.Q.F. Carbon Capture from CO₂-Rich Natural Gas via Gas-Liquid Membrane Contactors with Aqueous-Amine Solvents: A Review. *Gases* **2022**, *2*, 98–133. <https://doi.org/10.3390/gases2030007>

Academic Editor: Paola Ammendola

Received: 2 July 2022

Accepted: 17 August 2022

Published: 1 September 2022

Publisher's Note: MDPI stays neutral with regard to jurisdictional claims in published maps and institutional affiliations.



Copyright: © 2022 by the authors. Licensee MDPI, Basel, Switzerland. This article is an open access article distributed under the terms and conditions of the Creative Commons Attribution (CC BY) license (<https://creativecommons.org/licenses/by/4.0/>).

1. Introduction

The global population is continuously increasing, and it is foreseen that it will exceed 10 billion by 2050 [1]. In this scenario, natural gas (NG) exploration and production attract interest in meeting the growing world energy demand [2]. Moreover, NG plays a key role in the transition to renewable energy sources [3] as NG is the cleanest fossil fuel due to its high hydrogen/carbon ratio [4].

Proven NG reserves around the world are approximately 196.9 trillion cubic meters [4], but onshore NG reserves—with simpler production that is closer to consumers—are decreasing, while offshore NG reserves far from the coast and in deep waters are growing [5]. In this regard, oil production with associated NG in deep-waters and ultra-deep-waters usually presents high carbon dioxide (CO₂) content and gas-to-oil ratio, which entail difficulties for gas processing in offshore rigs where there are weight/footprint limitations [6]. Due to complex logistics for NG production/transportation in the context of deep-water offshore rigs, high costs lead to significant offshore CO₂-rich NG reserves being left unexplored. Albeit the existence of efficient technologies for onshore NG production, innovative low-cost technologies are necessary for deep-waters processing of CO₂-rich NG [5].

The concept of carbon capture utilization and storage (CCUS) is necessary to allow a smooth transition from fossil energy to renewable energy to keep a profitable industrial operation. In CO₂-rich NG processing, CO₂ removed from NG is transported to a storage

site [7]. Promising CO₂ utilizations are enhanced oil recovery (EOR) in oil-and-gas reservoirs [8] or enhanced gas recovery (EGR) in gas reservoirs [9]. In CCUS-EOR or CCUS-EGR, CO₂ is injected into reservoirs to increase oil and gas production. If the increase is high enough, the extra revenues can offset CO₂ capture/transportation costs entailing profits [7].

1.1. Natural Gas Purification Requirements

Raw NG primarily contains methane (CH₄) and secondarily ethane, propane, butanes, and heavier hydrocarbons. Other common constituents are CO₂, hydrogen sulfide (H₂S), water (H₂O), nitrogen (N₂), and trace components. Raw NG purification is necessary to meet gas pipeline specifications and market/environment regulations [10].

NG processing usually comprises: (i) H₂S removal [11]; (ii) water dew-point adjustment (WDPA) via dehydration [12]; (iii) hydrocarbon dew-point adjustment (HCDPA) [10]; and (iv) CO₂ removal. H₂S causes pipeline/equipment corrosion, it is undesirable in combustion, and threatens human health and the environment [11]. WDPA is necessary mainly because water condensed from NG may form solid gas-hydrates under high-pressure and low-temperature typically found in subsea pipelines [12]. HCDPA is necessary to avoid hydrocarbon condensation in pipelines (safety and efficiency issues) and to recover valuable NG liquids [13]. Besides, HCDPA removes hydrocarbons to meet the heating value specification (Wobbe Indexes), ensuring adequate gas-turbine and combustion equipment operations minimizing emissions [5]. Finally, CO₂ content is reduced to 2–3 mol%, increasing NG heating value, preventing solid CO₂-hydrates, avoiding corrosion, and avoiding occupying pipeline capacity with inert [14].

1.2. Carbon Capture from CO₂-Rich NG

Several technologies exist for carbon capture from CO₂-rich NG. Pressure-swing adsorption (PSA) prescribes selective CO₂ adsorption onto solid adsorbents at high-pressure conjugated with low-pressure CO₂ desorption [15]. PSA issues comprehend the methane purity-recovery tradeoff [16] and the low-pressure CO₂ release entailing compression costs [17].

Cryogenic distillation is considered for CO₂ ≥ 10 mol% due to lesser energy consumption and footprint compared to chemical absorption [18]. However, since cryogenic distillation operates at temperatures below the CO₂ triple-point [19], there is a risk of CO₂ freeze-out (dry-ice) inside the equipment, causing blockage [18]. Moreover, high-pressure cryogenic columns are protected against pressure surges by blowdown valves, which under cryogenic conditions can lead to dry-ice formation via the Joule–Thomson effect [20].

In offshore CO₂-rich NG processing, membrane permeation (MP) is adopted due to its low footprint, modularity, and flexibility to feed composition changes [21] and is recommended for high CO₂ content NG [22]. However, thanks to its capacity-selectivity tradeoff [23], permeate methane losses are remarkable, and the low-pressure CO₂-rich permeate imposes high compression costs [24].

Physical absorption (PhA) prescribes a physical solvent that dissolves CO₂ at high-pressure [25], requiring high CO₂ fugacity for high CO₂ loadings [26]. PhA is much less energy-intensive for solvent regeneration compared to chemical absorption at the expense of a low-pressure CO₂ stripping [6]. PhA drawbacks comprise (i) low CO₂/CH₄ selectivity entailing CH₄ losses in the stripped gas; (ii) low-pressure stripped gas entailing compression costs for EOR destination.

The most mature technology for CO₂ and H₂S removal from CO₂-rich NG is chemical absorption (ChA), which is based on CO₂ reactions with aqueous-alkanolamine solvents [27]. Aqueous-monoethanolamine (aqueous-MEA) and aqueous-methyl-diethanolamine (aqueous-MDEA) are the most used chemical solvents [28]. The main advantage is the high CO₂/CH₄ selectivity in a wide range of operation pressures [27] and this selectivity is particularly high at low CO₂ fugacity [22]. ChA generally operates with packing columns that have beds of variously-shaped packings—e.g., Pall rings or Berl saddles—providing a high specific surface area for CO₂ transfer. Packing columns are fed with lean solvent at the top

and with raw NG at the bottom in countercurrent flows [29]. ChA drawbacks comprise: (i) high heat-ratio ($\text{kJ}/\text{kg}^{\text{CO}_2}$) solvent regeneration [28]; (ii) solvent degradation (oxidation and thermal degradation) causing corrosion and efficiency loss; (iii) low-pressure CO_2 stripping entailing compression costs for EOR; (iv) hydraulic issues (e.g., foaming, channeling, flooding and entrainment) [29].

The gas-liquid membrane contactor (GLMC) combines MP and ChA advantages—without the respective drawbacks—becoming a promising solution for CO_2 -rich NG decarbonation [30]. In GLMC, the hollow-fiber membrane (HFM) provides a non-dispersive gas-liquid contact avoiding packing-columns hydraulic problems like foaming, channeling, flooding, and entrainment [31]. Comparatively, with MP, the selective chemical solvent and thousands of HFM inside the GLMC shell ensure high CO_2/CH_4 selectivity with low CH_4 loss, high mass transfer area per shell, compactness, modularity, and easy scale-up, all desired attributes for CO_2 removal from CO_2 -rich NG with aqueous-amine solvents in offshore rigs [22]. Comparatively, with conventional CO_2 absorption packing columns, GLMC reaches reductions up to 70% and 66% in size and weight, respectively [32]. Angular indifference is another advantage of GLMC vis-à-vis the sway of floating offshore rigs [33].

1.3. Review Articles on GLMC: Highlights and Gaps

An overview with an appreciation of typical GLMC reviews is conducted. Table 1 condenses reviews on GLMC aspects and developments, while Table 2 condenses reviews on post-combustion carbon capture GLMC, which, despite being somewhat outside the scope—as operating conditions are different from NG processing counterparts—is kept in the analysis due to common particularities of both scenarios (e.g., isothermal modeling issues and low-pressure CO_2 stripping GLMC). Table 3 analyzes general reviews on GLMC CO_2 removal from NG.

Table 1. Review articles: GLMC aspects and developments.

Description	Reference
GLMC environmental applications.	Mansourizadeh et al. [30]
HFM and solvent developments for CO_2 absorption.	Kim et al. [34]
New membranes, solvents, and GLMC configurations.	Li et al. [35]
Membrane development.	Xu et al. [36]
GLMC applications.	Babin et al. [37]
Membrane pore wetting in CO_2 capture with GLMC.	Ibrahim et al. [38]
GLMC acid-gas removal.	Zhang and Wang [39]

Table 2. Review articles: GLMC post-combustion carbon capture.

Description	Reference
Comparisons of GLMC models.	Rivero et al. [40]
GLMC operation and models; highlighted the need for non-isothermal GLMC modeling with water interfacial transfer.	Zhao et al. [41]
CO_2 stripping GLMC modeling, including state-of-the-art GLMC; solvent selection based on experiments.	Vadillo et al. [42]
GLMC modeling (no critical analysis).	Zhang et al. [43]
GLMC modeling (no critical analysis).	Cui and deMontigny [44]
Isothermal GLMC modeling with chemical reaction; cited eight articles with isothermal GLMC modeling.	Li and Chen [45]

Table 3. Review articles: GLMC CO₂ removal from CO₂-rich NG.

Description	Reference
Isothermal GLMC modeling without energy balances and assuming ideal gas behavior; poorly discussed head-loss calculation.	Ng et al. [46]
Comparison of technologies for offshore rigs: ChA, GLMC, rotating packed-bed, ultrasonic reactor, microchannel reactor.	Tay et al. [29]
Comparison of state-of-the-art MP and GLMC.	Siagian et al. [24]
MP and GLMC for acid-gas removal and NG dehydration in offshore rigs.	Dalane et al. [47]
GLMC applications, including H ₂ S removal from NG.	Bazhenov et al. [48]
Comprehensive review on solvent selection for GLMC NG decarbonation.	Shokrollahi et al. [25]
Ionic-liquid solvents for CO ₂ /H ₂ S removal from NG; experimental and design studies to make ionic-liquid solvents as effective as aqueous-amine solvents.	Karadas et al. [49]
Simplified isothermal GLMC modeling: ideal gas behavior, low pressure, and Henry's law for CO ₂ vapor-liquid equilibrium (VLE). Out-of-date.	Mansourizadeh and Ismail [50]

1.4. The Present Work

This work intends to fill the gaps in common reviews on GLMC for NG decarbonation and solvent regeneration seen in Table 3. Common deficiencies of Table 3 reviews comprehend: (i) lack of rigorous high-pressure non-isothermal GLMC modeling; (ii) lack of rigorous estimation of thermodynamic properties under multi-reactive conditions; (iii) lack of consideration of thermal and compressibility effects under chemical reactions; and (iv) GLMC implementation in professional process simulators.

In this context, this work critically reviews experimental and theoretical GLMC studies focusing on two applications: (i) CO₂ removal from CO₂-rich NG considering high-pressure operation and H₂O/H₂S handling and (ii) low-pressure CO₂ stripping for solvent regeneration. Section 2 reviews studies on GLMC principles, materials and configurations. Section 3 addresses experimental studies on the two mentioned applications. Section 4 critically reviews GLMC modeling for the two mentioned applications, including GLMC implementation in professional process simulators, analyzing model simplifications and limitations. Future prospects and concluding remarks are the object of Section 5.

2. GLMC: Principles, Materials, and Configurations

GLMC is modular equipment configured in batteries. Each GLMC module contains thousands of hydrophobic HFM tubes fixed into a shell-and-tube arrangement [51] in Figure 1. Equipment inclination translates into GLMC angular indifference [33].

GLMC is configurable as an absorber (for CO₂ capture) or as a stripper (CO₂ stripping for solvent regeneration). In both cases, GLMC has two feeds (where L is the molar flowrate of the GLMC liquid stream and V is the gas counterpart): (i) GLMC-absorber: NG feed ($V_{absorber}^{in}$); lean aqueous-amine solvent ($L_{absorber}^{in}$) [52]; (ii) GLMC-stripper: Sweep-gas (nitrogen [53] or steam [54]) ($V_{stripper}^{in}$); rich aqueous-amine solvent ($L_{stripper}^{in}$).

GLMC modules can operate with parallel V and L flows (co-current contact) [55] or opposed V and L flows (counter-current contact) [56]. Whichever the case, V flows inside HFM tubes or on the shell-side, while L respectively flows on the shell-side or inside HFM tubes. Consequently, there are four different GLMC configurations shown in Figure 1: (a,b) apply counter-current contact; (c,d) apply parallel contact; (a,c) have L in shell-side and V inside HFM tubes; (b,d) have L inside HFM tubes and V in shell-side [57]. Since HFM is a physical barrier against phase dispersion, additional phase separation equipment is not necessary [37]. HFM also increases the interfacial area reducing equipment size [58].

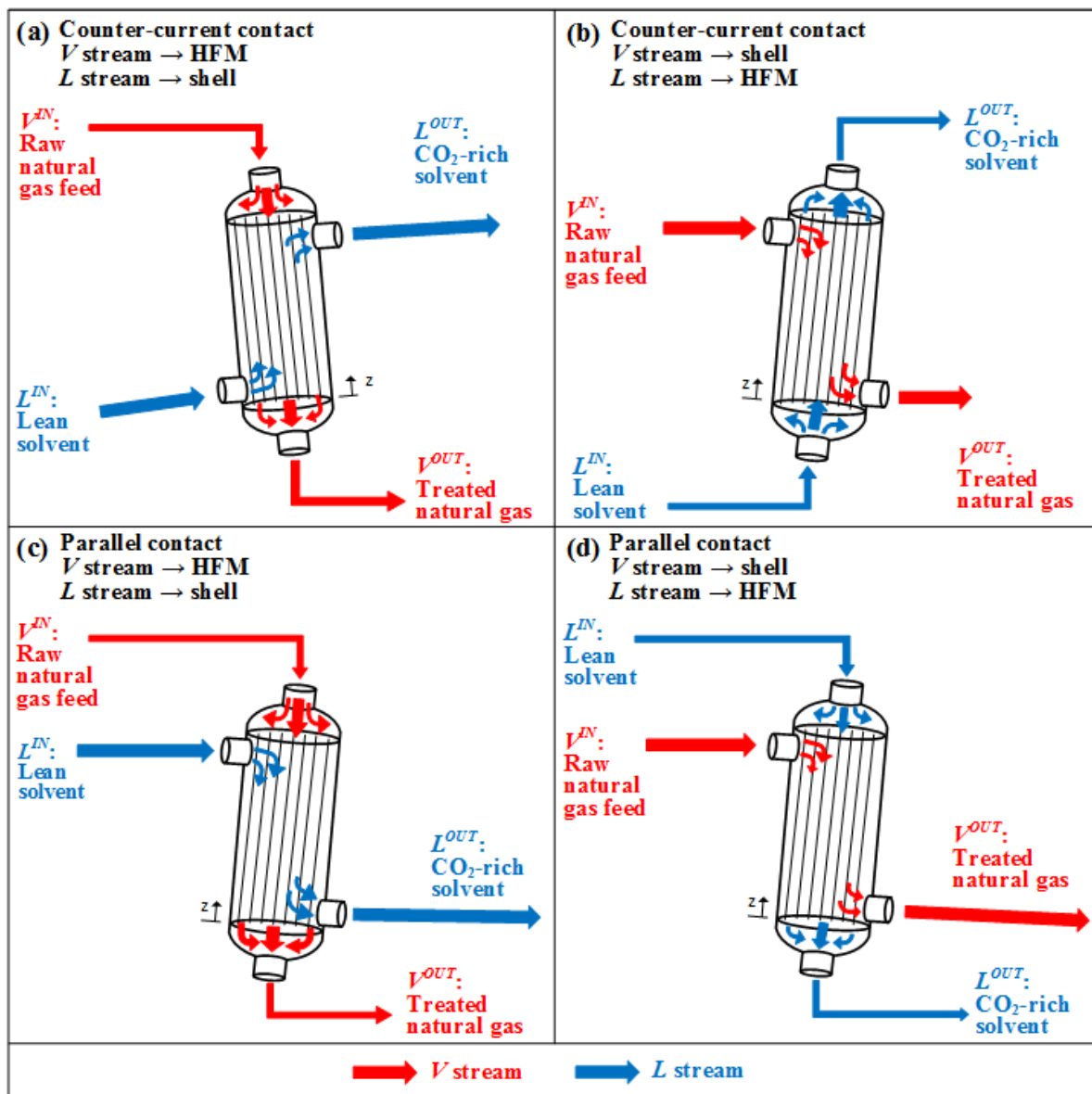


Figure 1. GLMC setups: Counter-current contact: (a) HFM:V, Shell:L; (b) HFM:L, Shell:V. Parallel contact: (c) HFM:V, Shell:L; (d) HFM:L, Shell:V.

GLMC is based on reactive-vapor-liquid-equilibrium (RVLE) since V and L streams are kept in direct contact through the HFM pores and relatively rapid chemical reactions occur in the liquid. In GLMC-absorber with chemical solvent, high CO_2/CH_4 selectivity is imposed by the aqueous solvent thanks to CH_4 hydrophobicity [33] and selective CO_2 conversion via liquid phase chemical reactions. When crossing the membranes, CH_4 rapidly reaches its low solubility in the aqueous solvent, such that CH_4 bubbles as a small vapor phase may form on the liquid side. As absorption chemical reactions between the solvent and CO_2 (or H_2S) are exothermic, the liquid temperature continuously increases, reducing CH_4 solubility and raising CH_4 fugacity over the liquid. Therefore, an L stream can be a single-phase liquid or a two-phase stream. Moreover, the CH_4 bubbles on the solvent side contribute to stripping some $\text{CO}_2/\text{H}_2\text{S}$ from the solvent, at the same time raising trans-membrane transport via reduction of $\text{CO}_2/\text{H}_2\text{S}$ fugacities in the liquid [33].

On the other hand, in GLMC-absorber with physical solvent, CO_2 does not react with the solvent, so species mass transfers and CO_2/CH_4 selectivity depend only on gas

diffusivities into the solvent and solute solubilities in the solvent. In this case, CO₂ Henry's Law is frequently used for VLE predictions [59].

In GLMC, convective heat transfers occur due to temperature differences between (i) *V* and *L* streams across HFM; (ii) shell-side phase and shell outside. As molar isobaric heat capacity (\bar{C}_P) values imply $V\bar{C}_{P_V} \ll L\bar{C}_{P_L}$, the *L* stream controls the temperature distribution; consequently, *L* and *V* temperature difference is near zero $|T_V - T_L| \approx 0$ at a given GLMC axial position due to convective interfacial heat transfer.

Water can transfer *L*→*V* or *V*→*L*, depending on the interfacial difference of H₂O fugacities $\hat{f}_{V_{H_2O}} - \hat{f}_{L_{H_2O}}$, influenced by the water content of feeds and absorption heat effects. For counter-current GLMC, the lowest T_V , T_L values occur at the *L* inlet, which is also the *V* outlet position. As *V* approaches its outlet at water saturation, its temperature lowers and condensation can occur, turning *V* into a two-phase flow [33]. Additionally, the large absorption heat release can vaporize solvent on the *L* side [60]. Considering all these thermal effects, both *L* and *V* can be single-phase or two-phase streams at some GLMC point [33].

GLMC-stripper regenerates physical solvents (*L*) with nitrogen or steam as sweep-gas (*V*). A vacuum-driven pump can also be employed to reduce *V* pressure. Since CO₂/H₂S fugacities in the sweep-gas are lower than in the solvent, CO₂/H₂S move *L*→*V* enabling separation without heat supply [54]. As Figure 2 shows, CO₂/H₂S move *V*→*L* in GLMC-absorber and *L*→*V* in GLMC-stripper, while H₂O moves *V*→*L* or *L*→*V* whether $\hat{f}_{V_{H_2O}} - \hat{f}_{L_{H_2O}} > 0$ or $\hat{f}_{V_{H_2O}} - \hat{f}_{L_{H_2O}} < 0$. N₂ transfer in GLMC-stripper is negligible since N₂ is highly hydrophobic [53].

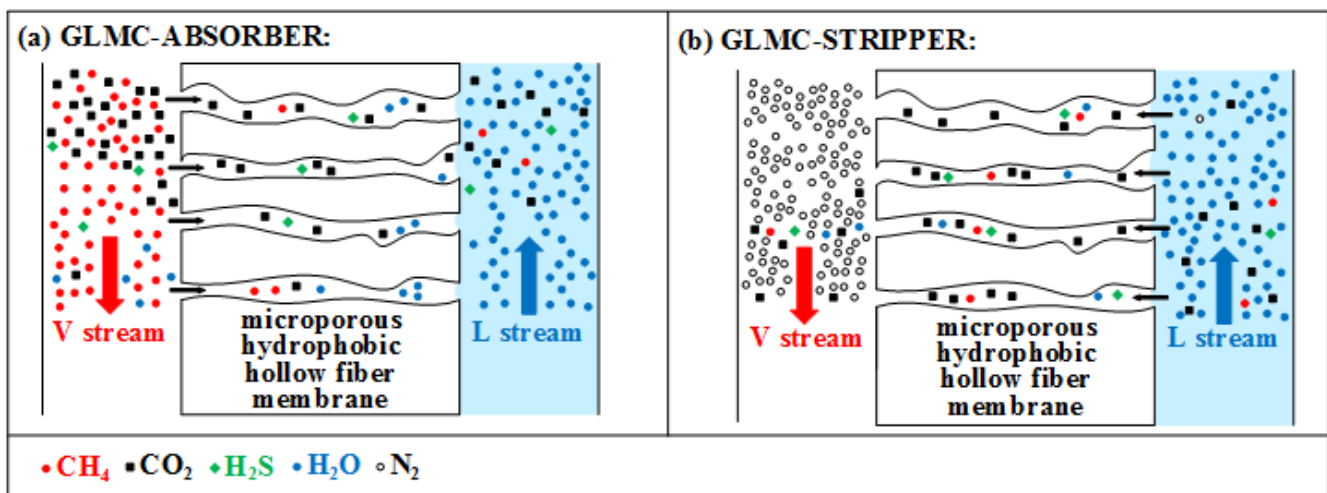


Figure 2. Multicomponent mass transfers: GLMC-absorber (a); GLMC-stripper (b) (H₂O can move *V*→*L* or *L*→*V*).

2.1. HFM for GLMC

Contrarily to MP, which uses dense selective membranes, GLMC adopts non-selective microporous HFM to allow *V*-*L* contact and selectivity is imposed by the solvent [61]. Figure 3 depicts how HFM works as a mass transfer barrier preventing phase dispersion [62]. Figure 3a represents direct *V*-*L* contact in tray columns or packing columns with phase dispersion. Figure 3b shows microporous HFM with gas-filled pores ensuring *V*-*L* contact with low mass transfer resistance [63]. However, during GLMC operation, the solvent may fill the pores (Figure 3c), increasing mass transfer resistance drastically and reducing transfer fluxes. This undesirable phenomenon compromises GLMC performance and is called membrane pore wetting (MPW) [62]. MPW is influenced by membrane characteristics (pores diameter, tortuosity, porosity, surface roughness), solvent surface tension, and operating conditions, while some solvents may favor MPW by affecting HFM

hydrophobicity, morphology, and roughness. To avoid MPW, HFM material must be hydrophobic such as polypropylene (PP), polyvinylidene fluoride (PVDF), polytetrafluorethylene (PTFE), polyether ether ketone (PEEK), and solvents should have high surface tension, negligible vapor pressure and should not chemically attack HFM [41]. Figure 3d shows another solution against MPW wherein dense HFM CO₂ permeable and solvent impermeable are used. However, dense HFM presents high transfer resistance and does not fit in the original GLMC concept of non-dispersive V-L contact [62]. A compromise solution uses composite HFM (Figure 3e) consisting of an ultrathin dense skin layer onto microporous support. The ultrathin layer is generally a fluorine-based hydrophobic material, while the microporous support—made of a cheaper material like PP—should be mechanically resistant, chemically stable, and highly porous to minimize transfer resistance [62].

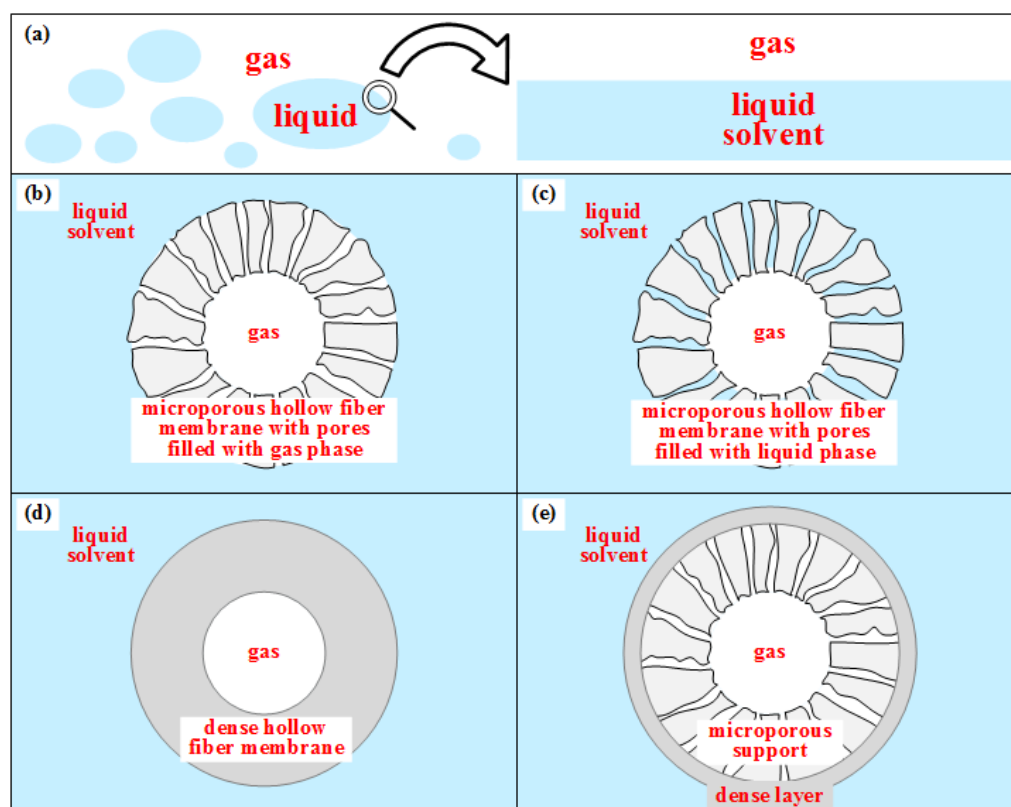


Figure 3. HFM as a barrier for mass transfer without phase dispersion: (a) direct V-L contact with phase dispersion; (b) microporous HFM V-L contact with gas-filled pores; (c) microporous HFM V-L contact with liquid-filled pores; (d) Dense HFM without V-L contact; (e) Composite HFM without V-L contact.

2.2. Solvents for GLMC CO₂ Absorption

Hereafter, physical and chemical GLMC solvents are discussed.

2.2.1. Physical Solvents

PhA relies on CO₂ solubility, which follows Henry's law, such that the absorption loading is favored by high CO₂ fugacity and low temperature. Thus, PhA can perform CO₂ removal from high-pressure raw NG. Comparatively to ChA, the main PhA advantage is the lower heat ratio for solvent regeneration [64]. Physical solvents are listed in Table 4 for GLMC CO₂ removal from NG.

Table 4. Physical solvents proposed for GLMC CO₂ removal from NG.

Physical Solvent	Reference
Water	[65]
Propylene carbonate (Fluor™ process)	[66]
Dimethyl ethers of propylene glycol (DEPG) (Selexol™ process)	[67]
Chilled methanol (Rectisol™ process)	[68]
N-methyl-2-pyrrolidone (NMP) (Purisol™ process)	[26]
Ionic-liquid	[69]

Some promising GLMC physical solvents are ionic liquids, which are salts of organic cations with organic anions. Ionic liquids exhibit melting points below 100 °C, negligible vapor pressure, high CO₂ solubility, and thermal stability but present high viscosity as a disadvantage [70].

2.2.2. Chemical Solvents

ChA is characterized by high CO₂/CH₄ selectivity and limited absorption loadings (kg^{CO₂}/kg^{Solvent}), both due to chemical reactions of the solvent with CO₂. Aqueous-amine solvents are the most used in ChA for CO₂ capture from NG due to high reactivity, low cost, easy regeneration and high CO₂/CH₄ selectivity [71]. Aqueous-MEA, aqueous-DEA (aqueous-diethanolamine) and aqueous-MDEA are examples of aqueous-amine solvents extensively employed for NG decarbonation since 1930 [72]. However, aqueous-amines exhibit drawbacks such as high heat-ratio (kJ/kg^{CO₂}) solvent regeneration, thermal/oxidative degradation, corrosiveness and limited CO₂ loading [73].

Aqueous-MEA is the most used for ChA CO₂ capture, exhibiting high reactivity at low-pressure or high-pressure [74], while aqueous-MDEA is adequate at high pressure despite lower absorption rate [75], which recommends using reactivity promoters. Table 5 lists literature studies on chemical solvents for GLMC NG decarbonation.

Table 5. Chemical solvents investigated for GLMC CO₂ removal from NG.

Chemical Solvents	Reference
Primary amines	
Aqueous-MEA	[76]
Aqueous-DGA (Aqueous-Diglycolamine)	[77]
Secondary amines	
Aqueous-DEA	[78]
Aqueous-DIPA (Aqueous-Diisopropanolamine)	[79]
Aqueous-PZ (Aqueous-Piperazine)	[80]
Aqueous-EMEA (Aqueous-N-ethyl-monoethanolamine)	[81]
Tertiary amines	
Aqueous-TEA (Aqueous-Triethanolamine)	[80]
Aqueous-MDEA	[82]
Sterically hindered amines	
Aqueous-AMP (Aqueous-2-amino-2-methyl-1-propanol)	[83]
Alkali-salts	
Aqueous-K ₂ CO ₃	[84]
Alkali	
Aqueous-NaOH	[85]
Amino-acid salts	
Aqueous-AAS	[86]

2.2.3. Solvent Blends

The literature presents CO₂ capture studies (for GLMC or not) with several blended solvents [87], namely: (i) aqueous-MDEA-PZ (PZ promoter) [88]; (ii) aqueous-MEA-MDEA, aqueous-MEA-DIPA and several combinations of aqueous-amines [89]; (iii) aqueous-PZ-K₂CO₃ (PZ promoter) [90]. Physical and chemical solvents are also blended, such as NMP with aqueous-ethanolamine [26] and ionic-liquid with aqueous-ethanolamine [91].

3. Experimental Studies: GLMC NG Decarbonation

Experimental studies exclusively on NG decarbonation involving GLMC-absorber and GLMC-stripper are reviewed, while studies on GLMC modeling from experiments are left to Section 4.

3.1. Experiments on GLMC CO₂ Absorption from NG

Qi and Cussler [92] started an investigation of HFM-GLMC in 1985 via experiments with CO₂ transfer in the liquid, followed by gas-to-liquid transfer across HFM [93]. They unveiled the advantages of HFM-GLMC over packing columns: the higher GLMC transfer area overcomes the HFM mass transfer resistance.

Dindore et al. [94] screened combinations of HFM and physical solvents for GLMC CO₂ capture by testing eight physical solvents with five HFM materials. Since few combinations were compatible, the authors demonstrated the importance of HFM-solvent compatibility to avoid MPW and its higher mass transfer resistance. The authors suggested the combination of propylene carbonate solvent with microporous PTFE-HFM or microporous PP-HFM, highlighting the high PTFE cost.

Atcharyawut et al. [95] studied CO₂ separation from CO₂+CH₄ gas mixtures in the GLMC shell-side with several solvents—water, aqueous-NaOH-NaCl, and aqueous-MEA—flowing inside HFM, evincing superiority of counter-current contact over parallel contact. Low CO₂/CH₄ selectivity was found and justified by the small GLMC module used. The operating pressure was not clearly informed, but it seems that low pressures were used.

Hedayat et al. [96] investigated GLMC for H₂S and CO₂ capture from NG with aqueous-MDEA, aqueous-DEA-MDEA, and aqueous-MEA-MDEA solvents. The blend aqueous-DEA-MDEA did not provide any benefit over aqueous-MDEA, and it was observed that MEA preferably reacts with CO₂ and MDEA with H₂S. The best capture efficiencies were obtained with the aqueous-MEA-MDEA blend. The experiments were conducted at low pressures and are not representative of real NG processing conditions.

Al-Marzouqi et al. [97] experimentally evaluated different HFMs and solvents for CO₂ removal from CO₂+CH₄ mixtures with CO₂ = 10 mol%. Among the tested HFM, PP-HFM reached the best performance, while among the tested aqueous-amines, aqueous-TEPA (aqueous-tetraethylenepentamine), aqueous-TETA (aqueous-triethylenetetramine) and aqueous-DETA (aqueous-diethylenetriamine) reached better CO₂ removal rates comparatively to aqueous-MEA, aqueous-DEA, and aqueous-EDA (aqueous-ethylenediamine). Aqueous-NaOH presented higher CO₂/CH₄ selectivity than aqueous-MEA. Again, experiments were conducted at low pressure.

Marzouk et al. [98] was the first work with high-pressure (P = 50 bar) GLMC experiments on CO₂ removal from NG (CO₂ = 9.5 mol%, CH₄ = 90.5 mol%). Expanded polytetrafluoroethylene (ePTFE) microporous HFM was used and physical and chemical solvents—water, aqueous-NaOH, and aqueous-MEA—were evaluated. Results showed that the positive effect of increasing gas pressure is much more pronounced in physical solvents than in chemical solvents; i.e., physical solvents are suitable at high-pressure, while chemical solvents can work at low-pressure. Despite the need for investigations on H₂S removal and simultaneous CO₂-H₂S removal from NG at high pressure, experiments considered only CO₂ removal due to the risks of H₂S experiments. Soon after, Marzouk et al. [99] modified the experimental setup to investigate high-pressure (P = 50 bar) H₂S removal from NG (H₂S = 2 mol%, CH₄ = 98 mol%) using the same HFMs and solvents from [98], finding H₂S removal results similar to the CO₂ removal results of [98]. Posteri-

orly, Marzouk et al. [100] investigated GLMC simultaneous CO₂-H₂S removal from NG (CO₂ = 5 mol%, H₂S = 2 mol%, CH₄ = 93 mol%) at high-pressure (P = 50 bar) with same solvents of [98], and comparing ePTFE and PFA (poly(tetrafluoroethylene-co-perfluorinated alkyl vinyl ether)) as HFM. PFA-HFM presented CO₂ and H₂S transmembrane fluxes ≈10 times higher than ePTFE-HFM counterparts, entailing transfer area reductions of 10 times in PFA-GLMC modules.

Rahim et al. [86] compared GLMC CO₂ absorption/stripping performances of four amino-acid salts (AAS) aqueous solvents with aqueous-MEA and aqueous-NaOH, showing that aqueous-AAS had the best CO₂ stripping performance as it just depends on pH changes. Albeit aqueous-NaOH reached the best absorption results, this solvent cannot be regenerated via ordinary CO₂ stripping, while aqueous-MEA can be regenerated but presented the worst CO₂ removal performance. However, all solvents were tested at 0.5 mol/L, while it is well-known that aqueous-MEA is better at 30 w/w% or ≈5 mol/L (i.e., ten-fold higher MEA composition). Apparently, the authors used very diluted aqueous-MEA to “establish” the superiority of aqueous-AAS.

Al-Marzouqi et al. [101] performed GLMC experiments to explore operating conditions for CO₂ capture from NG (CO₂ = 5 mol%, CH₄ = 95 mol%) at high-pressure (P = 50 bar) considering PFA-HFM and aqueous-NaOH, aqueous-DEA and aqueous-K₂CO₃ in long-term bench-scale runs. Pilot-scale tests were recommended.

Afterward, Hatab et al. [85] presented a contribution to the literature as, for the first time, spherical glass beads were investigated as additional packing in the solvent shell-side to create turbulence improving mass transfer. GLMC experiments were carried out for CO₂ removal from NG (CO₂ = 5 mol%, CH₄ = 95 mol%) using aqueous-NaOH and aqueous-amine solvents at pressures up to P = 25 bar. This work attracted attention as it proved the role of baffles in GLMC shell-side, an aspect frequently ignored. Transverse baffles can also lead to GLMC intensification.

Kang et al. [88] investigated GLMC CO₂ removal from CO₂-rich NG (45 mol%–70 mol% CO₂) at high-pressure (1 bar–60 bar) with PVDF-HFM and aqueous-MDEA-PZ as solvent. The CO₂ removal efficiency was enhanced by increasing pressure or transfer area or reducing feed flowrate at the expense of increasing the CH₄ loss rate.

Kartohardjono et al. [102] evaluated polyethyleneglycol-300 solvent for GLMC CO₂ capture from CO₂-CH₄ gas mixture (CO₂ = 30 mol%, CH₄ = 70 mol%). Albeit the solvent is not well-known, operational conditions were badly informed, and only obvious conclusions were drawn without relevant novelties.

The novelty in Ghobadi et al. [103] is the demonstration that smaller HFM diameters favor GLMC CO₂ separation. Low-pressure experiments were conducted with aqueous-MEA, aqueous-DEA, aqueous-TEA, and water solvents for CO₂ removal from the CO₂-CH₄ gas mixture (CO₂ = 2.5 mol%, CH₄ = 97.5 mol%). Aqueous-MEA was considered the best solvent.

Chan et al. [104] questionably affirmed that GLMC is disadvantageous in comparison with packing columns for NG processing due to the higher GLMC solvent/gas ratio for CO₂ removal. Works were cited to justify this claim in which low CO₂ loadings were obtained with aqueous-amine solvents. However, Chan et al. [104] eventually discovered that just increasing GLMC module length (i.e., increasing transfer area) proved to be sufficient to solve the problem.

Petukhov et al. [105] reviewed GLMC CO₂/H₂S removal from NG with PP-HFM and aqueous-NaOH as solvent. Experiments were also conducted at a low-pressure range (1.5–8 bar) for CO₂/H₂S removal from CH₄-CO₂-H₂S gas feeds, which suggests that this study contemplates biogas purification. However, attention was not given to ChA thermal effects.

Hosseini et al. [106] proposed mass transfer intensification by applying vibration to GLMC to induce turbulence. Experiments at P = 1.5 bar were conducted with pure CO₂ and aqueous potassium glycinate 15 w/w% as solvent.

3.2. Experiments on GLMC CO₂ Stripping

The closed-loop combination of GLMC-absorber for CO₂ removal from NG with GLMC-stripper for CO₂ stripping is a low-weight and low-footprint promising solution for offshore NG processing. Mansourizadeh [107] conducted experiments on GLMC CO₂ absorption/stripping using water solvent in a closed loop, with pure CO₂ feed and pure N₂ stripping gas.

GLMC CO₂ stripping from ionic-liquid solvent has also been studied. Lu et al. [108] studied aqueous ionic-liquid solvents 1-butyl-3-methyl-imidazolium tetrafluoroborate ([bmin][BF₄]) and 1-(3-aminopropyl)-3-methyl-imidazolium tetrafluoroborate ([apmin][BF₄]) for coupled GLMC CO₂ absorption and GLMC solvent regeneration applying vacuum for CO₂ stripping. Aqueous-[bmin][BF₄] was completely regenerated, while aqueous-[apmin][BF₄] presented a difficult regeneration. Mulukutla et al. [109] investigated ionic-liquid [bmin][DCA] with 20 w/w% polyamidoamine for GLMC CO₂ capture and GLMC solvent regeneration showing that the stripped gas attained 92 mol% CO₂. Bazhenov et al. [110] proved the concept of high-pressure CO₂ stripping from ionic-liquid [Emin][BF₄] via moderate pressure-swing ($\Delta P = 10$ bar) coupled to temperature-swing. [Emin][BF₄] is recommended for pre-combustion CO₂ removal and NG sweetening with GLMC absorption/stripping. Simons et al. [111] described an experimental setup for testing ionic-liquid solvents for GLMC CO₂ absorption/stripping and demonstrated it with 50 w/w% aqueous dimethyl-propylenediamine acetates.

The majority of experiments on GLMC CO₂ stripping were conducted with aqueous-MEA since it is the most used solvent for GLMC CO₂ removal from CO₂-rich NG. Koonaphadeelert et al. [112] investigated CO₂ stripping from aqueous-MEA with ceramic HFM GLMC as this operation is performed preheating CO₂-rich aqueous-MEA at $T = 100$ °C, at which most polymeric HFM cannot withstand. Khaisri et al. [113] employed PTFE-HFM at the same conditions as [112], observing that increasing temperature and MEA content increase CO₂ stripping, but too high MEA contents decrease CO₂ transfer due to high viscosity. Khaisri et al. [114] presented a similar work using a similar GLMC-stripper experimental setup. Scholes et al. [115] tested three HFM at a temperature range of 70 °C–105 °C, confirming higher CO₂ stripping fluxes at higher temperatures and higher Reynolds numbers as turbulence decreases boundary layer mass transfer resistance. Scholes et al. [54] tested steam as a stripping agent for CO₂ stripping from aqueous-MEA. Kianfar et al. [116] investigated polysulfone (PSF) as HFM for GLMC-absorber and GLMC-stripper. CO₂ stripping was performed at $T = 80$ °C and $P = 0.5$ bar with a pure N₂ stripping agent. Lee et al. [117] developed a vacuum-driven stripping method at $P = 61.325$ kPa. Comparatively to the common N₂ sweep-gas stripping, this process reduces heat consumption, increasing stripping efficiency and CO₂ purity due to N₂ absence.

Experimental studies of CO₂ stripping from aqueous-DEA focused on HFM development and adopted N₂ as stripping gas at $T = 80$ °C. Naim et al. [118] prepared different PVDF-HFM with LiCl as a non-solvent additive. It was observed that increasing HFM LiCl content increases mass transfer performance. Naim et al. [119] tested LiCl, glycerol, polyethylene-glycol (PEG400), methanol, and H₃PO₄ non-solvent additives to PVDF-HFM, showing that PVDF-PEG400-HFM presented the highest CO₂ transfer flux. Naim and Ismail [120] confirmed the potential of polyetherimide (PEI) HFM, while Naim et al. [121] compared PVDF-HFM with PEI-HFM. Both were prepared with polyethylene-glycol (PEG) incorporation and PVDF-PEG-HFM presented a higher CO₂ transfer flux. Rahbari-Sisakht et al. [122] developed a PVDF-HFM with surface modifying molecules. Hosseini and Mansourizadeh [123] investigated microporous hydrophobic poly(vinylidene fluoride-co-hexafluoropropylene) (PVDF-HFP) HFM.

Aqueous-MDEA-PZ for GLMC CO₂ absorption/stripping was studied by Akan et al. [124], showing that vacuum-driven CO₂ stripping was achieved at $T = 92$ °C using helium as stripping gas. Rahim et al. [125] evaluated PVDF-HFM GLMC CO₂ stripping from different solvents: aqueous-MEA, aqueous-DEA, aqueous-AMP, and aqueous potassium glycinate. For all solvents, the authors demonstrated that mass transfer increases by

increasing temperature and initial CO₂ content. Wang et al. [126] investigated aqueous solutions of 16 amines via fast screening experiments to find the solvents with lower heat-ratio for CO₂ stripping in a combined GLMC absorption/stripping process. In terms of overall performance, aqueous-MDEA was recommended for GLMC-stripper.

Finally, Kim et al. [127] investigated the microporous and hydrophobic electrospun poly(vinylidene fluoride-co-hexafluoro propylene) nanofiber membrane for CO₂ stripping from aqueous potassium glycinate.

4. Modeling Studies: GLMC NG Decarbonation

The development of accurate GLMC modeling is of great importance as it avoids spending money and time on experiments as well as providing the necessary information to predict and analyze GLMC performance [128]. This section presents an extensive critical review of GLMC modeling for CO₂ removal from NG and for CO₂ stripping. Throughout Section 4, Tables 6–8 are cited in order to present mathematical relationships related to the works and models under discussion. As Tables 6–8 naturally belong to the context of Section 4.3, they are installed there.

4.1. GLMC Modeling for CO₂ Absorption from NG

As NG decarbonation is performed at high-pressure and frequently with concentrated aqueous-amine solvents highly deviating from ideal solution behavior, rigorous thermodynamic models must be used for property prediction, comprising an Equation-of-State (EOS) for the vapor phase and an activity coefficient model for the liquid phase. Moreover, mass, heat, and momentum transfers occur simultaneously and influence each other; i.e., related predictions must be accurate to ensure reliability in industrial scale conditions. Moreover, the multicomponent mass transfer must be considered as CO₂/H₂S simultaneous removal is necessarily entailing unavoidable transfers of CH₄ and other hydrocarbons. Besides, H₂O can move in both directions, $V \rightarrow L$ or $L \rightarrow V$.

Dindore et al. [129] modeled CO₂/H₂S mass transfer with chemical reaction in a cross-flow GLMC with aqueous-K₂CO₃ solvent. The model is simplified and does not include energy balance and thermal effects. Experiments were carried out with a CO₂-H₂S-N₂ gas mixture which deviates from NG behavior as CH₄ is considerably more soluble than N₂. Therefore CO₂/CH₄ selectivity and CH₄ losses were not evaluated.

The GLMC models for CO₂ removal from NG of Al-Marzouqi et al. [65] (Table 7, Equations (47), (48), (50), (51), (53), (55) and (56)) with water solvent and Al-Marzouqi et al. [130] (Table 7, Equations (47), (48), (50), (51), (53), (55) and (56)) with aqueous-MEA and aqueous-NaOH were developed for low-pressure GLMC. Faiz and Al-Marzouqi [131] presented a low-pressure GLMC model (Table 7, Equations (47), (50) and (55)) based on reaction kinetics for H₂S absorption in aqueous-Na₂CO₃, which is not suitable for high-pressure NG processing. Furthermore, NG purification requires CO₂/H₂S simultaneous removal. Faiz and Al-Marzouqi [76] developed a low-pressure model (Table 7, Equations (47), (48), (50), (51), (53), (55)–(60)) for CO₂/H₂S simultaneous removal with aqueous-MEA. Keshavarz et al. [78] presented a simplified GLMC model (Table 7, Equation (55), Table 8, Equation (68)) for CO₂/H₂S simultaneous removal from CO₂-H₂S-N₂ gas mixture (CO₂ = 15 mol%, H₂S = 5 mol%, N₂ = 80 mol%) with aqueous-DEA. Unfortunately, low-pressure and isothermal behavior was considered an unrealistic situation in high-pressure CO₂/H₂S absorption from NG with aqueous-amines, which is a highly exothermic process. In addition, ideal gas behavior was also assumed.

Faiz and Al-Marzouqi [132] developed the first GLMC modeling study at high-pressure ($P < 50$ bar) for CO₂ removal from NG considering water and aqueous-amine solvents. The model (Table 7, Equations (47), (48), (50), (51), (53), and (55)–(57)) consisted of differential equations in cylindrical coordinates for CO₂ mass transfer solved with COMSOL software and was validated with Marzouk et al. [98] experiments. GLMC transfers of H₂S, CH₄, and water were not taken into account. The authors justified neglecting CH₄ transfer due to the low CH₄ solubility in aqueous solutions. However, this assumption is

problematic because with physical solvents at high-pressure, CH₄ losses can reach 9–10%, while with chemical solvents, CH₄ losses are considerably smaller but never negligible. In addition, this model does not prescribe energy balance and head-loss calculations; i.e., heat effects and temperature/pressure changes were not predicted. Posteriorly, Faiz and Al-Marzouqi [133] presented a low-pressure isothermal GLMC model (Table 7, Equations (47), (48), (50), (51), (53), (55), and (56)) for CO₂/H₂S simultaneous removal from NG with aqueous-K₂CO₃ solvent. The authors implemented two serial GLMC modules to favor reaction kinetics so that all the H₂S and a small portion of CO₂ are removed in module #1 and the remaining CO₂ is removed in module #2. However, this low-pressure isothermal model is not compatible with real NG processing conditions.

Faiz et al. [134] proposed a GLMC model (Table 7, Equations (47), (48), (50), (51), (53), and (55)–(57)) taking into account the gas velocity change in the axial direction as CO₂ is removed from the gas initially with 10 mol% CO₂. The model was validated with experiments of [97] and showed, for high CO₂ content in the gas feed, that the effect of gas velocity change is more evident since the gas velocity decreases significantly. The decrease in gas velocity implies a higher residence time, entailing higher CO₂ capture. Model predictions were in better agreement with the experimental data for chemical solvents, but they were not good for physical solvents. This study also contemplates a low-pressure GLMC NG purification.

Rezakazemi et al. [82] studied CO₂/H₂S simultaneous GLMC removal from NG using aqueous-MDEA as solvent. A two-dimensional model was proposed (Table 7, Equations (48), (51)–(53), (55), and (56)), considering axial and radial diffusion, convection, chemical reactions, and momentum equations. The model was solved with CFD techniques. However, the model was developed at low-pressure and ambient temperature, entailing oversimplified assumptions; namely: (i) isothermal GLMC profiles are unrealistic in a system with exothermic reactions of CO₂ with concentrated aqueous-MDEA; (ii) ideal gas behavior is not adequate at real operating conditions of high-pressure NG sweetening. The authors affirm that CH₄ does not dissolve in the solvent; another unrealistic outcome and water mass transfer was also ignored.

Boributh et al. [135] developed a 1D GLMC model (Table 6, Equation (37)) with water solvent for estimating the mass transfer area considering different GLMC module arrangements: single-stage module, two-stage parallel modules, two-stage serial modules with the separated liquid flow, and two-stage serial modules with combined liquid flow. In Boributh et al. [136] (Table 6, Equation (37)), the GLMC with water solvent model includes the effect of pore size distribution to predict MPW and CO₂ mass transfer correctly. Boributh et al. [137] proposed a GLMC model (Table 6, Equation (37)) for the design of multistage GLMC schemes with aqueous-MEA solvent. Works [135–137] modeled counter-current GLMC CO₂ removal from CO₂-CH₄ gas mixtures considering partial MPW. These works are similar, performed low-pressure case studies, and presented the same GLMC modeling simplifications: isothermal conditions, ideal gas behavior, and zero head-loss.

A new GLMC concept is found in Cai et al. [138], which proposed to carry out both the acid-gas absorption and solvent regeneration in a single step, i.e., in the same GLMC cross-flow modules. The aim is to save space in offshore processing plants. In this concept, the solvent flows on the shell-side, while two types of HFM are used in the module. CO₂-rich NG flows in the microporous HFM at high-pressure ($P = 50$ bar), wherein CO₂/H₂S absorptions take place at the gas-liquid interface. Inside the GLMC module, there is also dense HFM, kept at low-pressure ($P = 1$ bar) so that the difference of pressure in relation to the solvent generates a stripping driving force which promotes solvent regeneration in the shell-side as CO₂/H₂S scape to the low-pressure HFM. Therefore, CO₂/H₂S absorption and solvent regeneration occur simultaneously in the GLMC module, theoretically resulting in better absorption efficiency as the solvent is kept with low acid-gas content while flowing through the GLMC module. The authors also suggest using baffles to improve mass transfer efficiency by increasing turbulence. Propylene carbonate was the physical solvent as it presents better CO₂ solubility in comparison with water. The use of physical solvents

is recommended as chemical solvents demand heat-intensive regeneration and require more space on offshore rigs. Indeed, it is easy to understand that this GLMC concept would never work with chemical solvents because chemical solvents would necessarily require a GLMC-absorber and a separate solvent regeneration step. The GLMC model considers isothermal mass transfers through the microporous HFMs, through the dense HFMs, and on the shell side. The authors assumed isothermal conditions and neglected gas head-losses. Despite the new concept, this work did not trigger analogous works by other authors since then.

An important and disruptive contribution comes from Ghasem et al. [60], as it was the first model to consider GLMC water vaporization and the respective heat effect, a phenomenon systematically ignored in the GLMC modeling literature, which prefers to assume isothermal GLMC modeling without water mass transfer, a fact that Ghasem et al. proved to be unrealistic. In [60], GLMC CO₂ absorption from NG was performed using an aqueous-NaOH solvent. In comparison with previous works, a more complete GLMC model was developed (Table 7, Equations (47), (49)–(51), (54), (56), and (61)–(67)). Instead of considering isothermal GLMC and neglecting pressure drop, the model [60] considers mass, energy, and momentum balances. The work carried out experiments and results were compared with model predictions. Nonetheless, experiments were performed at atmospheric pressure with a raw NG composition of 10 mol% CO₂ and 90 mol% CH₄. Besides, in real NG processing, the high-pressure raw NG is water-saturated, so that water can transfer in both directions, a fact not considered in [60]. Moreover, real raw NG contains H₂S and light hydrocarbons (C₂⁺).

After the good work in [60], Ghasem et al. [139] published a badly written article with several typos, including the article title and the titles of some sections. CO₂ absorption from NG was investigated experimentally and theoretically with a GLMC model comprising only material balances (Table 7, Equations (47), (48), (51), (53), and (56)). Aqueous potassium glycinate was compared with aqueous-amine solvents showing superior results, a questionable outcome. The article is a mess: the text creates confusion among MEA, DEA, and MDEA all the time. Thereby, it is impossible to be sure of which aqueous-amine solvents were investigated.

A complete GLMC thermodynamic model is found in de Medeiros et al. [33], which simulated an offshore high-pressure NG purification process for GLMC CO₂ removal with aqueous-MEA-MDEA. The GLMC model comprises a new acid-gas, water, and alkanolamines equilibrium model (AGWA model) [140] capable of reproducing chemical absorption and desorption of CO₂ (and H₂S) in aqueous-amines, over a wide range of pressures, which was calibrated in terms of equilibrium constants with AGWA VLE data from the literature. The real species VLE is superimposed on the multi-reactive chemical equilibrium for the formation of fictitious species (non-ionic and non-volatile complexes), defining a reactive VLE or RVLE [140]. The GLMC *V* and *L* flows are parallel and unidimensional (1D), assuming compressible two-phase plug-flow for *V* and *L* streams. The model also considered the mass transfer of CH₄, H₂O, and light hydrocarbons and was developed through rigorous mass, energy, and momentum balances for *V* and *L* streams, allowing heat and mass interfacial transfers, with shear and compressibility terms, and all properties of all phases rigorously calculated by the Peng–Robinson EOS (PR-EOS) and Soave–Redlich–Kwong EOS (SRK-EOS). This model was able to reproduce several interesting behaviors along the GLMC length as profiles of both streams, such as molar flowrates, species compositions, temperatures, pressures, fugacities, and CO₂/CH₄ selectivity [33]. Model equations are shown in Equations (1) to (7).

Trans-membrane fluxes of real species “*k*”:

$$N_k^{flux} = \Pi_k * (\hat{f}_{V_k} - \hat{f}_{L_k}) \quad (1)$$

Real species EMWR (Equivalent Moles Without Reaction) mass balances for V and L streams:

$$\frac{dV_k}{dz} = -Sa * N_k^{flux} \quad (2)$$

$$\frac{dL_k}{dz} = Sa * N_k^{flux} \quad (3)$$

where N_k^{flux} are trans-membrane fluxes of real species “k”; Π_k are trans-membrane mass transfer coefficients of species “k”; \hat{f}_{V_k} and \hat{f}_{L_k} are the V and L fugacities of real species “k”; Sa is the interfacial area per length; V_k and L_k are V molar flowrate and the L EMWR molar flowrate of real species “k.”

Momentum balances for V and L:

$$\left\{ \Gamma_{T_V} * (v_V)^2 \right\} \frac{dT_V}{dz} + \left\{ \Gamma_{P_V} * (v_V)^2 - 1 \right\} \frac{dP_V}{dz} + \sum_k^{n_{RS}} \left\{ \Gamma_{V_k} * (v_V)^2 \right\} \frac{dV_k}{dz} = \rho_V g * \text{sen}\theta - \left(\frac{v_V}{S_V} \right) qSa + \psi_V \left(\frac{\Pi D + Sa}{S_V} \right) \quad (4)$$

$$\left\{ \Gamma_{T_L} * (v_L)^2 \right\} \frac{dT_L}{dz} + \left\{ \Gamma_{P_L} * (v_L)^2 - 1 \right\} \frac{dP_L}{dz} + \sum_k^{n_{RS}} \left\{ \Gamma_{L_k} * (v_L)^2 \right\} \frac{dL_k}{dz} = \rho_L g * \text{sen}\theta + \left(\frac{v_L}{S_L} \right) qSa + \left(\frac{v_L - v_V}{S_L} \right) qSa + \psi_L \left(\frac{Sa}{S_L} \right) \quad (5)$$

where D is the GLMC shell internal diameter, θ is GLMC inclination, g is the gravity acceleration, n_{RS} is the number of real species, Γ_{T_V} and Γ_{T_L} are isobaric expansivity of V and L at RVLE, Γ_{P_V} and Γ_{P_L} are isothermal compressibility of V and L at RVLE, Γ_{V_k} and Γ_{L_k} are species “k” mol expansivity of V and L at RVLE, T_V and T_L are V and L temperatures, P_V and P_L are V and L absolute pressures, v_V and v_L are V and L flow velocities, ρ_V and ρ_L are V and L densities, S_V and S_L are sections of V and L flows, ψ_V and ψ_L are the shear stress on contact surfaces in V and L flows.

Energy balances for V and L:

$$\left\{ \frac{\rho_V \bar{C}_{P_V}}{M_V} - \Gamma_{T_V} (v_V)^2 \right\} \frac{dT_V}{dz} + \left\{ 1 + \frac{T_V}{\rho_V} \Gamma_{T_V} - \Gamma_{P_V} (v_V)^2 \right\} \frac{dP_V}{dz} - \sum_k^{n_{RS}} \left\{ \Gamma_{V_k} * (v_V)^2 \right\} \frac{dV_k}{dz} = \left(\frac{v_V}{S_V} \right) qSa - \rho_V g * \text{sen}\theta + \frac{\Omega_E \Pi D \rho_V}{q_V} (T^{amb} - T_V) - \left(\frac{\Omega_I Sa \rho_V}{q_V} \right) (T_V - T_L) \quad (6)$$

$$\left\{ \frac{\rho_L \bar{C}_{P_L}}{M_L} - \Gamma_{T_L} (v_L)^2 \right\} \frac{dT_L}{dz} + \left\{ 1 + \frac{T_L}{\rho_L} \Gamma_{T_L} - \Gamma_{P_L} (v_L)^2 \right\} \frac{dP_L}{dz} - \sum_k^{n_{RS}} \left\{ \Gamma_{L_k} * (v_L)^2 \right\} \frac{dL_k}{dz} = - \left(\frac{v_L}{S_L} \right) qSa - \rho_L g * \text{sen}\theta + \left(\frac{\Omega_I Sa \rho_L}{q_L} \right) (T_V - T_L) + \left(\frac{Sa \rho_L}{q_L} \right) \sum_k^{n_{RS}} N_k^{flux} \left(\bar{E}_{V_k} - \bar{E}_{L_k}^{EMWR} \right) \quad (7)$$

where \bar{C}_{P_V} and \bar{C}_{P_L} are V and L molar isobaric heat capacities, M_V and M_L are the V and L EMWR molar masses, q_V and q_L are V and L mass flowrates, q is the HFM mass flux, Ω_E and Ω_I are external and internal heat transfer coefficients, T^{amb} is the outside temperature, \bar{E}_{V_k} and $\bar{E}_{L_k}^{EMWR}$ are the PMP^{EMWR} energies of “k” in V and L.

Faiz et al. [141] described a 2D GLMC model (Table 7, Equations (48), (50), (51), (53), and (55)–(57)) for H₂S removal from high-pressure NG with water solvent. Model predictions agreed perfectly with the experimental data only at low pressures. At high pressures, agreement with experimental data only occurred when the “pseudo-wetting” condition (3%) (MPW) was assumed. The model ignores the transfer of other species, energy balances, and head losses.

Razavi et al. [79] modeled low-pressure GLMC CO₂ removal from NG with an aqueous di-isopropanol amine (DIPA) solvent. The 2D GLMC model (Table 7, Equations (47), (48), (50)–(53), (55), and (56)) ignores thermal effects (isothermal GLMC), assumes ideal gas behavior, and considers only species mass balances without head-loss calculations.

Cai et al. [142] modeled crossflow GLMC for CO₂ removal from NG. Experiments were performed and a CFD modeling was solved with ANSYS software. The model considers

mass and momentum balances, without energy balance, in three-dimensional geometry. The study considered carbon capture from pure CO₂ with water solvent at $P = 1$ atm and $T = 298$ K, which are distant values from real NG processing conditions.

Abdolahi-Mansoorkhani and Seddighi [80] investigated HFM improvements with the incorporation of montmorillonite nanoparticles for CO₂ removal from CO₂-CH₄ mixtures (CO₂ = 10 mol%, CH₄ = 90 mol%) using aqueous-MEA, aqueous-PZ, aqueous-TEA, and aqueous-EDA solvents. A 2D finite element modeling in cylindrical coordinates predicted GLMC behavior (Table 7, Equations (47), (48), (50)–(53), and (55)–(60)). Despite the highly exothermic ChA with aqueous-amines, the model ignores energy balances, considering isothermal profiles without head-loss, ideal gas behavior, and VLE via Henry's law. Besides, only CO₂ is transferred.

Nakhjiri et al. [143] conducted experiments and developed a two-dimensional (2D) GLMC model (Table 7, Equations (47), (48), (50), (51), (53) and (55)–(57)) for prediction of CO₂ removal from CO₂-CH₄ mixtures (CO₂ = 30 mol%, CH₄ = 70 mol%) with aqueous-MEA and aqueous-TEA. Predicted results were compared with experimental counterparts in both non-wetting and partial wetting (MPW) modes of operation. Model differential equations were solved with COMSOL software. This work did not unveil any noticeable novelty, as the isothermal low-pressure 2D model was developed with simplifications found in previously published works such as ideal gas behavior, Henry's law for VLE, absence of H₂S and H₂O in raw NG, only CO₂ transference, and no head-loss. Nakhjiri et al. [144] used almost the same equations (Table 7, Equations (47), (48), (50), (51), (53), and (55)–(60)) of [143], with the inclusion of aqueous-NaOH experiments, finding the following order of CO₂ removal performances: aqueous-MEA > aqueous-NaOH > aqueous-TEA. Model predictions were compared with data from [95]. Nakhjiri and Heydarinasab [145] studied GLMC CO₂ removal from a CO₂-CH₄ gas mixture (CO₂ = 10 mol%, CH₄ = 90 mol%) with aqueous ethylenediamine (EDA), aqueous 2-(1-piperazinyl)-ethylamine (PZEA) and aqueous potassium sarcosinate (PS) solvents using a model (Table 7, Equations (47), (48), (50)–(53) and (55)–(57)) similar to [143,144] models, considering non-wetting mode of operation. Model predictions were compared with data from [65] for validation, an awkward procedure since the experiments from [65] were conducted with pure water solvent. Posteriorly, Nakhjiri et al. [84] slightly improved their previous GLMC model [143] by considering simultaneous CO₂/H₂S removal with aqueous-K₂CO₃ solvent, including momentum balance equations (Table 7, Equations (47), (48), (50), (51), (53), (55)–(57) and (61)–(64)). However, all the remaining simplifications of [143–145] were kept.

Mesbah et al. [90] presented a theoretical study of GLMC CO₂ removal from CO₂-CH₄ gas mixtures using an aqueous-K₂CO₃ solvent containing a 2-methylpiperazine (2MPZ) promoter. Despite considering a complex chemical reaction scheme of CO₂ with aqueous-K₂CO₃-2MPZ, the 2D GLMC model (Table 7, Equations (47), (48), (50)–(53) and (55)–(57)) is simplified with the following assumptions: isothermal profiles, low-pressure, ideal gas behavior, Henry's law VLE, and only CO₂ is transferred. Awkwardly, the supposed model validation was performed with experimental data from [143], which involved only aqueous-MEA and aqueous-TEA solvents.

Fougerit et al. [146] performed an experimental and modeling study of GLMC CO₂ removal from CO₂-CH₄-H₂O gas mixtures covering a wide range of CO₂ contents, namely: NG sweetening (CO₂ = 5–10 mol%), post-combustion carbon capture (CO₂ = 10–15 mol%), biogas upgrading (CO₂ = 35–50 mol%). However, the authors ignored that each feed mixture needs different process conditions. Besides, the 1D mass transfer model is simplified: only CO₂ transference is considered, isothermal GLMC, ideal gas behavior, and low-pressure ($P = 5.0$ bar).

The GLMC decarbonation of coal-bed methane, an NG abundant in China, was studied by Zhang et al. [147] with a 2D GLMC model (Table 7, Equations (48), (50), (51), (53) and (55)–(57)) considering aqueous-MEA, aqueous-DEA, aqueous-TEA and aqueous 1-(2-hydroxyethyl)pyrrolidine solvents. The GLMC model is also simplified: low-pressure, ideal gas behavior, and isothermal GLMC profiles were adopted for ChA with aqueous-amine

solvents. Pan et al. [148] adopted the same GLMC model (Table 7, Equations (48), (50), (51), (53), (55), and (56)) for the simultaneous CO₂/H₂S removal from coal-bed methane using aqueous-K₂CO₃ with potassium lysinate (PL) solvent. The pressure influence in the range 1 bar–50 bar on CO₂/H₂S transfers was studied (still under ideal gas behavior).

Ghasem [149] experimentally studied GLMC CO₂ absorption from CO₂-CH₄ mixtures (CO₂ = 10 mol%, CH₄ = 90 mol%) and also the CO₂ stripping from the solvent. The solvent was 0.5 mol/L aqueous potassium glycinate in a closed loop with N₂ as stripping gas. Experimental results were compared with predictions of a GLMC model, which is 2D axisymmetric and transient, considering CO₂/CH₄ transports in GLMC-absorber, and CO₂/N₂ transports in GLMC-stripper. The model is simplified: it considers low-pressure, ideal gas behavior, isothermal profiles, VLE via Henry's law, and lacks energy balance and head-loss calculations. H₂S and H₂O are absent. Ghasem [150] investigated the influence of HFM bore size on the highly exothermic CO₂ removal from NG with aqueous-MEA, considering VLE via Henry's law. In comparison with [149], it was used a similar low-pressure 2D GLMC model at steady-state (Table 7, Equations (47), (48), (50), (51), (53), (55) and (56)).

GLMC Modeling with Professional Process Simulators for CO₂ Removal from NG

Implementation of GLMC modeling for carbon capture from NG in professional process simulators is crucial for rigorous GLMC modeling due to more accurate thermodynamic properties estimation [128].

Among the few works implementing GLMC modeling in process simulators, there are studies on CO₂ removal from other sorts of gas streams (e.g., biogas and syngas). Kerber and Repke [151] studied GLMC biogas purification, while Villeneuve et al. [152,153] studied carbon capture from post-combustion flue gas with GLMC implementation in Aspen Custom Modeler. Usman et al. [154] developed a GLMC model for pre-combustion CO₂ capture in MATLAB. Posteriorly, Usman et al. [155] integrated the MATLAB code with the HYSYS process simulator through the Cape-Open simulation compiler.

There are just a few works on GLMC modeling in process simulators for CO₂ removal from NG. Hoff et al. [156] conducted laboratory-scale experiments on CO₂ removal from flue gas with aqueous-MEA and on high-pressure CO₂ removal from NG with aqueous-MDEA. The authors developed a 2D diffusion-reaction model to predict experimental absorption rates and concentration/temperature GLMC profiles. The model considers mass, energy, and momentum balances, and VLE was modeled via Henry's law with activity coefficients to account for liquid phase non-ideality. The model equations—shown in Equations (8) to (16)—were solved via MATLAB.

Gas mass balance equations:

$$\frac{dN_k^{flux}}{dz} = \frac{v_V}{RT_V} \frac{\partial P_V}{\partial z} + \frac{P_V}{RT_V} \frac{\partial v_V}{\partial z} - \frac{P_V v_V}{R(T_V)^2} \frac{\partial T_V}{\partial z} = \sum_k N_k^{flux} \frac{A_{SISA}}{\varepsilon_V} \quad (8)$$

$$\frac{dv_V}{dz} = \left(-\frac{v_V}{P_V} \frac{\partial P_V}{\partial z} \right) + \left(\frac{v_V}{T_V} \frac{\partial T_V}{\partial z} \right) - \left(\frac{RT_V}{v_V} N_k^{flux} \frac{A_{SISA}}{\varepsilon_V} \right) \quad (9)$$

$$\frac{dP_{V_k}}{dz} = \left(-\frac{P_{V_k}}{v_V} \frac{\partial v_V}{\partial z} \right) + \left(\frac{P_{V_k}}{T_V} \frac{\partial T_V}{\partial z} \right) - \left(\frac{RT_V}{v_V} N_k^{flux} \frac{A_{SISA}}{\varepsilon_V} \right) \quad (10)$$

$$\sum_k \bar{C}_{P_{V,k}} N_k^{flux} \frac{\partial T_V}{\partial z} = Q \quad (11)$$

where R is the ideal gas constant, A_{SISA} is the specific GLMC inner surface area, ε_V is the fraction of total area available to gas flow, $\bar{C}_{P_{V,k}}$ is the V molar isobaric heat capacity of species “ k ” and Q is the heat rate.

Trans-membrane mass flux of species “k”:

$$N_k^{flux} = \frac{(P_{V_k} - H_k C_{L_{k,m}})}{RT_V \left(\frac{1}{k_{k,V}} + \frac{r_o \ln(r_o/r_i)}{D_{k,m}^{eff}} \right)} + X_k \sum_k N_k^{flux} \quad (12)$$

$$D_{k,m}^{eff} = \frac{D_k \varepsilon}{\tau} \quad (13)$$

$$Q = \frac{1}{\left(\frac{1}{\Omega_V} + \frac{1}{\Omega_m} \right)} (T_V - T_{L,m}) \quad (14)$$

where P_{V_k} is the partial pressure of “k,” H_k is Henry’s law constant of “k,” $C_{L_{k,m}}$ is the concentration of “k” at the liquid–membrane interface, $k_{k,V}$ is the gas film mass transfer coefficient of “k,” r_i and r_o are the internal and external HFM radiuses, $D_{k,m}^{eff}$ is the effective membrane diffusivity of “k,” D_k is the molecular diffusivity of “k,” ε is membrane porosity, τ is membrane tortuosity, Ω_V is V heat transfer coefficient, Ω_m is the HFM heat transfer coefficient and $T_{L,m}$ is the temperature at liquid–membrane interface.

Transport model for the liquid phase based upon mass and energy conservation:

$$2v_L \left[1 - \left(\frac{r}{r_i} \right)^2 \right] \frac{\partial C_{L_k}}{\partial z} = D_k \left(\frac{1}{r} \frac{\partial C_{L_k}}{\partial r} + \frac{\partial^2 C_{L_k}}{\partial r^2} \right) + \frac{\partial D_k}{\partial r} \frac{\partial C_{L_k}}{\partial r} + R_k \quad (15)$$

$$2v_L \left[1 - \left(\frac{r}{r_i} \right)^2 \right] \bar{C}_{P_L} \rho_L \frac{\partial T_L}{\partial z} = \lambda_L \frac{1}{r} \frac{\partial}{\partial r} \left(r \frac{\partial T_L}{\partial r} \right) + R_k (-\Delta H_r) \quad (16)$$

where C_{L_k} is L molar concentration of “k,” R_k is the chemical reaction rate in terms of “k,” \bar{C}_{P_L} is the L molar isobaric heat capacity, λ_L is L thermal conductivity, and ΔH_r is the enthalpy of reaction.

Posteriorly, the model of Hoff et al. [156] was improved for utilization in process simulators, including new thermodynamic models for aqueous-MEA and aqueous-MDEA/PZ, and solvent flow modeling inside HFM or in shell-side, besides improvements for gas and solvent head-loss calculation. In Hoff and Svendsen [157], the GLMC model comprises an RVLE CO₂-water-amines system based on the Deshmukh–Mather approach [158], employing a modified Debye–Hückel model similar to Kuranov et al. [159]. The gas phase was modeled with PR-EOS and the trans-membrane fluxes were modified as shown in Equations (17) to (19).

$$N_k^{flux} = \frac{(\hat{f}_{V_k} - \hat{f}_{L_k})}{ZRT_V \left(\frac{1}{k_{k,V}} + \frac{1}{k_{k,m}} + \frac{H}{Ek_{k,L}} \right)} + X_k \sum_k N_k^{flux} \quad (17)$$

$$k_m = \frac{\varepsilon D_p}{\tau r_i \ln(r_o/r_i)} \quad (18)$$

$$D_p = \frac{1}{(1 - X_L) \left(\frac{1}{D_m} + \frac{1}{D_{Kn}} \right) + \left(X_L \frac{1}{D_{m,L}} \right)} \quad (19)$$

where Z , $k_{k,V}$, k_m , $k_{k,L}$, E , D_p , D_m , D_{Kn} , $D_{m,L}$, X_L are respectively, compressibility factor, gas film, membrane and liquid film mass transfer coefficients of “k,” enhancement factor, combined diffusivity, membrane diffusivity, Knudsen diffusivity, diffusivity of membrane at liquid phase and partial liquid penetration, respectively.

In Hoff and Svendsen [157], the following gas treatments were simulated: (i) low-pressure post-combustion carbon capture from offshore gas-turbines flue-gas to attain 90% capture with 30 w/w% aqueous-MEA in GLMC cross-flow modules installed in the process simulator SINTEF/NTNU CO2SIM; (ii) high-pressure ($P = 70$ bar) offshore sweetening of

NG (CO₂ = 10 mol%) to CO₂ = 2.5 mol% using 30 w/w% aqueous-MDEA in GLMC parallel-flow modules installed in the process simulator Protreat; (iii) high-pressure (P = 70 bar) offshore sweetening of NG (CO₂ = 10 mol%) to LNG specification of CO₂ = 50 ppm-mol using 30 w/w% aqueous-MDEA with 5 w/w% PZ in GLMC parallel-flow modules installed in the process simulator Protreat. In comparison with packing columns, total equipment volume can be reduced to 25% using GLMC with liquid on the shell side. With liquid flowing inside HFM, the advantage reduces significantly. Authors highlighted that GLMC may significantly improve offshore CO₂ capture from gas-turbine flue-gas and for NG sweetening but pointed out the doubtful advantage of GLMC for post-combustion carbon capture due to a large number of required GLMC modules and high head-losses of V and L streams.

Quek et al. [160] developed a predictive GLMC model for high-pressure NG sweetening. A temperature correction was calculated for the adiabatic GLMC to account for the ChA thermal effects. Model equations were implemented in gPROMS modeling language using a second-order centered finite difference scheme to discretize the differential equations. Model results attained good comparison with lab-scale experiments of CO₂ absorption from CH₄-CO₂ and N₂-CO₂ mixtures at P = 11 bar and from pilot-scale experiments on NG sweetening at P = 54 bar, both using 39 w/w% aqueous-MDEA with 5 w/w% PZ.

Quek et al. [161] indicated limitations of their work [160] since it fails to describe the gradual increase in temperature through the equipment, besides not considering solvent evaporation. Thus, an improvement of their GLMC model was carried out in [161] via combining 1D and 2D mass balance equations to include MPW. Real gas behavior is implemented via PR-EOS. The GLMC model is shown in Equations (20) to (26).

Gas mass balance:

$$\bar{v}_V(z) \frac{\partial \bar{C}_{V\text{CO}_2}(z)}{\partial z} = -2 \frac{\varepsilon D_{\text{CO}_2,V}}{\tau r_i} \left(1 - \frac{ZRT_V}{P_V} \right) \frac{\partial C_{V\text{CO}_2}(r_i^+, z)}{\partial r} \quad (20)$$

$$\frac{\partial \bar{v}_V(z)}{\partial z} = -2 \frac{\varepsilon D_{\text{CO}_2,V}}{\tau r_i} \left(\frac{ZRT_V}{P_V} \right) \frac{\partial C_{V\text{CO}_2}(r_i^+, z)}{\partial r} \quad (21)$$

Membrane-dry mass balance:

$$0 = \frac{\partial^2 C_{\text{CO}_2}(r, z)}{\partial r^2} + \frac{1}{r} \frac{\partial C_{\text{CO}_2}(r, z)}{\partial r} \quad (22)$$

Membrane-wet mass balance:

$$0 = \frac{\varepsilon}{\tau} D_{k,L} \left[\frac{\partial^2 C_{Lk}(r, z)}{\partial r^2} + \frac{1}{r} \frac{\partial C_{Lk}(r, z)}{\partial r} \right] + R_k(C_{Lk}(r, z)), \quad k \in \{\text{CO}_2, \text{solvent}\} \quad (23)$$

Liquid mass balance:

$$v_L(r) \frac{\partial C_{Lk}(r, z)}{\partial z} = D_{k,L} \left[\frac{\partial^2 C_{Lk}(r, z)}{\partial r^2} + \frac{1}{r} \frac{\partial C_{Lk}(r, z)}{\partial r} + \frac{\partial^2 C_{Lk}(r, z)}{\partial z^2} \right] + R_k(C_{Lk}(r, z)), \quad k \in \{\text{CO}_2, \text{solvent}\} \quad (24)$$

$$v_L(r) = 2\bar{v}_L \left(r_{shell}^2 - r_o^2 \right) \frac{r_{shell}^2 - r_o^2 + 2r_{shell}^2 \ln\left(\frac{r_o}{r_{shell}}\right)}{4r_o^2 r_{shell}^2 - r_o^4 - 3r_{shell}^4 - 4r_{shell}^4 \ln\left(\frac{r_o}{r_{shell}}\right)} \quad (25)$$

$$\bar{v}_L = \frac{F_L}{N_{HF} \Pi r_{shell}^2 (1 - \phi)} \quad (26)$$

where \bar{v}_V and \bar{v}_L are V and L average velocities, $\bar{C}_{V\text{CO}_2}$ is the average V concentration of CO₂, $D_{\text{CO}_2,V}$ is V CO₂ diffusivity, $D_{k,L}$ is L diffusivity of "k," r_{shell} is the outer radius of the virtual cylindrical domain around each HFM, r_1^+ is the gas-membrane interface at the

pore-side, F_L is L volumetric flowrate, N_{HF} is the number of HFM within GLMC module and φ is the fiber volume fraction (packing-ratio).

To predict solvent evaporation in counter-current GLMC [161], the authors assumed a water-saturated gas at the GLMC outlet and used Raoult's law to calculate H_2O content. However, there is some impertinency in this assumption, as the two premises for Raoult's law are: (i) ideal gas vapor phase at low-pressure; (ii) ideal solution liquid phase with chemically similar species. As the GLMC has a gas phase at high pressure in VLE with a non-ideal solution with high ionic interaction between species, it would be much more adequate to use an equation-of-state for vapor fugacities, besides an excess Gibbs free energy local composition model for aqueous electrolyte systems. At the end of the article, the authors admitted that Raoult's law is questionable. Moreover, an energy balance was performed [161], considering the heat losses of solvent evaporation. As there is an inaccuracy in solvent loss prediction, this step is probably also inaccurate. Moreover, Henry's law was employed to calculate liquid phase methane, ethane, and propane concentrations. These steps are shown in Equations (27) to (31).

V composition:

$$Y_k^{out} = X_k^{in} \frac{P_k^{sat}}{P_V}, k \in \{H_2O, solvent\} \quad (27)$$

Rate of solvent loss:

$$q_{V_k} = Y_k^{out} M_{V_k} \bar{v}_V(0) N_{HF} \Pi r_1^2 \frac{P_V}{ZRT_V} = X_k^{out} M_{V_k} \bar{v}_V(0) N_{HF} \Pi r_1^2 \frac{P_k^{sat}}{ZRT_V}, k \in \{H_2O, solvent\} \quad (28)$$

Energy balance:

$$F_L \rho_L C_{P_L} \frac{dT_L(z)}{dz} = N_{HF} \Pi r_1^2 \frac{\partial (\bar{v}_V(z) \bar{C}_{V_{CO_2}}(z))}{\partial z} \Delta H_r \quad (29)$$

L light hydrocarbons concentrations:

$$C_{L_k}^{out} = \frac{Y_k^{in} P_V}{H_k}, k \in \{CH_4, C_2H_6, C_3H_8\} \quad (30)$$

Light hydrocarbons loss rate:

$$q_{L_k}^{out} = C_{L_k}^{out} M_{L_k} F_L, k \in \{CH_4, C_2H_6, C_3H_8\} \quad (31)$$

where Y_k^{out} is V outlet mol fraction of " k ," X_k^{out} and X_k^{in} are L outlet/inlet mol fraction of " k ," P_k^{sat} is the saturation pressure of " k ," q_{V_k} is V mass flowrate of " k ," M_{V_k} is V molar mass of " k ," \bar{v}_V is V average velocity and C_{P_L} is L mass isobaric heat capacity.

Besides ignoring solvent head-loss [161], the authors tried to convince us that gas head-loss can be safely neglected. On the other hand, several researchers, including Hoff and Svendsen [157], proved exactly the opposite. The model was solved with gPROMS modeling language. Gas feed compositions were 20–24 mol% CO_2 in a N_2 - CO_2 mixture ($P = 54$ bar, $T = 293$ K) in lab experiments and 5–18 mol% CO_2 NG ($P = 54$ bar, $T = 298$ K) in pilot runs. Solvent was 37 w/w% aqueous-MDEA with 6 w/w% PZ ($P = 54.30$ bar, $T = 310$ – 313 K) in lab experiments and 39 w/w% aqueous-MDEA with 5 w/w% PZ ($T = 303$ – 308 K) in pilot runs.

Quek et al. [162] installed the GLMC model from [161] in the process simulator gPROMS to perform the techno-economic assessment of the complete process for high-pressure NG sweetening and low-pressure regeneration in a closed-loop. Simulations predicted CO_2 absorption and light hydrocarbons losses, solvent evaporation, besides process energy consumption. Results were compared with data from a pilot plant in Malaysia with reasonable agreement. Raw gas composition was $CO_2 = 5$ mol%, $CH_4 = 85$ mol%, $C_2H_6 = 7$ mol%, $C_3H_8 = 3$ mol% at $P = 54$ bar, $T = 298$ K, and the fresh solvent was

39 w/w% aqueous-MDEA with 5 w/w% PZ ($P = 54.3$ bar, $T = 303\text{--}308$ K). Two solvent regenerations were considered: regeneration in stripping columns or semi-regeneration in low-pressure flash separators. Posteriorly, the design and scale-up of a commercial-scale GLMC was conducted with a semi-lean solvent at raw gas composition $\text{CO}_2 = 24$ mol%, $\text{CH}_4 = 73$ mol%, $\text{C}_2\text{H}_6 = 2$ mol%, $\text{C}_3\text{H}_8 = 1$ mol% ($P = 54$ bar, $T = 298$ K), while the semi-lean solvent was 39 w/w% aqueous-MDEA with 5 w/w% PZ ($P = 54.3$ bar, $T = 318$ K). CO_2 content was abated from 24 mol% to 6.5 mol%, which the authors considered excellent as they recommended the semi-lean regeneration with low-pressure flash to reduce energy consumption. However, it is widely known that the CO_2 target for NG sweetening usually ranges from 2 to 3 mol% [14]; thereby, employing stripping columns for complete solvent regeneration is more adequate in this case.

Da Cunha et al. [128] performed a technical evaluation of GLMC CO_2 removal from CO_2 -rich NG using 30 w/w% aqueous-MEA through process simulations in Aspen HYSYS V8.8. The authors developed a GLMC model, with the driving force for CO_2 transfer predicted with CO_2 V and L fugacity differences, rigorously calculated with thermodynamic resources of Aspen HYSYS V8.8 provided by the Acid-Gas package [163] (based on Electrolyte-NRTL model) for liquid phase properties and PR-EOS for vapor properties [164]. GLMC model equations consist of a non-linear algebraic system in Equations (32) to (34) solved by Newton-Raphson Method.

$$N_k = \Pi_k A \left\{ \frac{(\hat{f}_{V\text{CO}_2}^{\text{in}} - \hat{f}_{L\text{CO}_2}^{\text{out}}) - (\hat{f}_{V\text{CO}_2}^{\text{out}} - \hat{f}_{L\text{CO}_2}^{\text{in}})}{\ln(\hat{f}_{V\text{CO}_2}^{\text{in}} - \hat{f}_{L\text{CO}_2}^{\text{out}}) - \ln(\hat{f}_{V\text{CO}_2}^{\text{out}} - \hat{f}_{L\text{CO}_2}^{\text{in}})} \right\} \quad (32)$$

$$N_k = L^{\text{out}} X_{\text{CO}_2}^{\text{out}} - L^{\text{in}} X_{\text{CO}_2}^{\text{in}} \quad (33)$$

$$N_k = V^{\text{in}} Y_{\text{CO}_2}^{\text{in}} - V^{\text{out}} Y_{\text{CO}_2}^{\text{out}} \quad (34)$$

where N_k is the trans-membrane transfer rate of component “ k ,” Π_k is the trans-membrane mass transfer coefficient of “ k ,” A is the transfer area of the GLMC battery, $\hat{f}_{V\text{CO}_2}$ and $\hat{f}_{L\text{CO}_2}$ are V and L CO_2 fugacities, Y_{CO_2} and X_{CO_2} are V and L CO_2 molar fractions, and V and L are molar flowrates.

To perform process simulations in HYSYS, the authors created a GLMC HYSYS Unit Operation Extension (GLMC-UOE), in a similar procedure to Arinelli et al. [165] for MP unit operation. GLMC-UOE was programmed in Visual Basic 6.0, which contains an HYSYS Type Library with commands to access HYSYS directly. After programming and compiling the code, an external DLL file was generated, which was installed through an EDF file as an available unit operation in the HYSYS palette usable in HYSYS flowsheets. The EDF file was programmed with the Aspen HYSYS Extension View Editor and also provided the GLMC-UOE property windows, where an HYSYS user interface is filled by the user with all the necessary simulation information. GLMC model equations were programmed to be solved by the Newton–Raphson Method.

GLMC-UOE [128] is worthy of note because its present version already represents a new unit operation GLMC, which is implemented within an up-to-date professional simulation environment using full thermodynamics to calculate fluid properties and fugacities of real liquid and gas phases. Moreover, GLMC-UOE can be integrated into processing flowsheets comprising several other unit operations offered in the HYSYS palette, eventually constituting very complex process flowsheets.

4.2. GLMC Modeling for CO_2 Stripping from the Solvent

Complete GLMC models for low-pressure CO_2 stripping from the solvent require the same framework of GLMC for CO_2 removal from NG, as described in the first paragraph of Section 4.1.

Some GLMC models were developed for CO_2 stripping from physical solvents. Mehdipourghazi et al. [166] investigated CO_2 stripping from the water via PVDF-HFM

GLMC. The 2D model (Table 7, Equations (48), (50)–(53), (55), and (56)) only considers isothermal CO₂ transfer. Lee et al. [167] also studied vacuum-driven GLMC CO₂ stripping from water through experiments and using a 1D GLMC model (Table 6, Equations (35)–(38)) to assess liquid flowrate, vacuum pressure, and pH. Bahlake et al. [168] investigated GLMC CO₂/H₂S simultaneous stripping from the water via a 3D modeling approach whose differential equations were solved with COMSOL software. Sohaib et al. [69] investigated two ionic liquids for post-combustion carbon capture via GLMC-absorber coupled to GLMC-stripper. A 2D dynamic model (Table 7, Equations (48), (50)–(53), (55), and (56)) was implemented based on low-pressure and low-temperature mass transfer equations. Vadillo et al. [169] developed a 1D-2D GLMC model (Table 7, Equation (55), Table 8, Equation (68)) for vacuum-driven regeneration of the ionic-liquid 1-ethyl-3-methylimidazolium acetate [emin][Ac] solvent considering isothermal conditions. The best operating conditions were achieved at P = 0.4 bar and T = 310 K.

The literature has an evident interest in GLMC CO₂ stripping from aqueous-MEA. Ghadiri et al. [170] used pure N₂ for CO₂ stripping in a GLMC modeling study. The 2D model (Table 7, Equations (48), (53) and (55)–(57)) assumed isothermal and steady-state conditions, only CO₂ transference, and VLE via Henry's law. CO₂ mass transfer predictions were compared with experimental data from [113], with reasonable agreement. To remove CO₂ from 20 w/w% aqueous-MEA at T = 353 K, Wang et al. [171] used vacuum-driven stripping with steam as a stripping agent on the shell side at P = 20 kPa. The 1D-2D model (Table 7, Equation (55), Table 8, Equation (68)) is based on a system of steady-state continuity equations for each species with simultaneous diffusion and chemical reaction, considering isothermal operation and VLE via Henry's law. Mohammed et al. [172] developed a 2D GLMC model (Table 7, Equations (48), (50)–(53), (55), and (56)) to investigate the effect of SiO₂ nanoparticles on CO₂ stripping from aqueous-MEA. Authors considered isothermal GLMC and VLE via Henry's law. No energy balances or head-loss calculations were performed.

Table 6. 1D GLMC models are not related to processing simulators.

Main Equations	References
V→L (positive direction by convention)	
Mass balance equations:	
$\frac{dV_k}{dz} = -N_{HF}\Pi d_o N_k^{flux}$	(35) [167,173,174]
$\frac{dL_k}{dz} = N_{HF}\Pi d_o N_k^{flux}$	(36) [167,173,174]
$N_k^{flux} = k_{k,ov}(C_{V_k} - C_{L_k}^*)$	(37) [135–137,167,173,174]
$\frac{1}{a_m k_{k,ov}} = \frac{1}{a_{ext} k_{k,V}} + \frac{1}{a_m k_{k,m}} + \frac{H_k}{a_{int} E k_{k,L}}$	(38) [167,174]
Energy balance equations:	
$\frac{dT_V}{dz} = -\frac{Q^{flux}}{C_{P_V} \sum_k V_k^{flux}}$	(39) [173,174]
$\frac{dT_L}{dz} = \frac{Q^{flux} + \sum_k N_k^{flux} \Delta H_{k,abs/evap} + N_{CO_2}^{flux} \Delta H_r}{C_{P_L} \sum_k L_k^{flux}}$	(40) [173]
$\frac{dT_L}{dz} = \frac{Q^{flux} + \sum_k N_k^{flux} \Delta H_{k,abs/evap}}{C_{P_L} \sum_k L_k^{flux}}$	(41) [174]
$Q^{flux} = U(T_V - T_L)$	(42) [173,174]
$\frac{1}{a_m U} = \frac{1}{a_{ext} \Omega_V} + \frac{1}{a_m \Omega_m} + \frac{1}{a_{int} \Omega_L}$	(43) [174]
Pressure drop calculation:	
Stream inside HFM (Hagen-Poiseuille equation):	
$\frac{dP_i}{dz} = -\frac{8\mu_i v_i}{(r_i)^2}$	(44) [173,174]
Stream in the shell-side (Happel equation):	
$\frac{dP_o}{dz} = -\mu_o v_o K_{koz}$	(45) [173,174]
$K_{koz} = \frac{8\varphi}{[2m(\frac{1}{\varphi}) - 3 + 4\varphi - \varphi^2](r_o)^2}$	(46) [173,174]

where: $k_{k,ov}$: overall mass transfer coefficient of "k" (m/s); Q^{flux} : heat flux (W/m²); V_k^{flux} : V molar flux of "k" (mol/s); $\Delta H_{k,abs/evap}$: enthalpy of absorption or vaporization (J/mol); L_k^{flux} : L molar flux of "k" (mol/s); U: overall heat transfer coefficient (W/(m².K)); Ω_L : L heat transfer coefficient (W/(m².K)); a_{ext} : external specific interfacial area (-); a_{int} : internal specific interfacial area (-); a_m : specific membrane area (-); P_i : Pressure of the stream inside HFM (bar); μ_i : Dynamic viscosity of the predominant phase inside HFM (Pa.s); v_i : Velocity of the stream at internal surface of HFM (m/s); P_o : Pressure in the shell-side (bar); μ_o : Dynamic viscosity of the predominant phase in the shell-side (Pa.s); v_o : Velocity of the stream at the external surface of HFM (m/s); K_{koz} : Kozeny factor (m⁻²).

Table 7. GLMC 2D models are not related to processing simulators.

Main Equations	References
Mass balance equations:	
Reaction rate:	
$R_k = k_r C_{L_k} C_{L_j}$	(47)
Shell-side with Happel free surface model for velocity distribution:	
$D_{k,o} \left[\frac{\partial^2 C_{k,o}}{\partial r^2} + \frac{1}{r} \frac{\partial C_{k,o}}{\partial r} + \frac{\partial^2 C_{k,o}}{\partial z^2} \right] + R_k = v_{z,o} \frac{\partial C_{k,o}}{\partial z}$	(48) @
$D_{k,o} \left[\frac{\partial^2 C_{k,o}}{\partial r^2} + \frac{1}{r} \frac{\partial C_{k,o}}{\partial r} + \frac{\partial^2 C_{k,o}}{\partial z^2} \right] + R_k = \frac{\partial}{\partial z} (v_{z,o} C_{k,o}) + \frac{1}{r} \frac{\partial}{\partial r} (r v_{r,o} C_{k,o})$	(49) @
$v_{z,o} = 2\bar{v}_{z,o} \left[1 - \left(\frac{r}{r_i} \right)^2 \right] \times \left[\frac{\left(\frac{r}{r_{shell}} \right)^2 - \left(\frac{r_o}{r_{shell}} \right)^2 + 2 \ln \left(\frac{r_o}{r} \right)}{3 + \left(\frac{r_o}{r_{shell}} \right)^4 - 4 \left(\frac{r_o}{r_{shell}} \right)^2 + 4 \ln \left(\frac{r_o}{r_{shell}} \right)} \right]$	(50)
$r_{shell} = r_o \sqrt{\frac{1}{\varphi}}$	(51)
$\varphi = 1 - N_{HF} \left(\frac{d_o}{D} \right)^2$	(52)
Inside HFM with velocity distribution by Newtonian laminar flow:	
$D_{k,i} \left[\frac{\partial^2 C_{k,i}}{\partial r^2} + \frac{1}{r} \frac{\partial C_{k,i}}{\partial r} + \frac{\partial^2 C_{k,i}}{\partial z^2} \right] + R_k = v_{z,i} \frac{\partial C_{k,i}}{\partial z}$	(53) #
$D_{k,i} \left[\frac{\partial^2 C_{k,i}}{\partial r^2} + \frac{1}{r} \frac{\partial C_{k,i}}{\partial r} + \frac{\partial^2 C_{k,i}}{\partial z^2} \right] + R_k = \frac{\partial}{\partial z} (v_{z,i} C_{k,i}) + \frac{1}{r} \frac{\partial}{\partial r} (r v_{r,i} C_{k,i})$	(54) #
$v_{z,i} = 2\bar{v}_{z,i} \left[1 - \left(\frac{r}{r_i} \right)^2 \right]$	(55)
Diffusion through gas-filled membrane pores:	
$D_{k,m} \left[\frac{\partial^2 C_{k,m}}{\partial r^2} + \frac{1}{r} \frac{\partial C_{k,m}}{\partial r} + \frac{\partial^2 C_{k,m}}{\partial z^2} \right] = 0$	(56)
$D_{k,m} = \frac{D_{k,i} \times \varepsilon}{\tau}$ or $D_{k,m} = \frac{D_{k,o} \times \varepsilon}{\tau}$	(57) \$
Diffusion through partially-wetted membrane pores:	
Gas – filled part : $D_{k,mV} \left[\frac{\partial^2 C_{k,mV}}{\partial r^2} + \frac{1}{r} \frac{\partial C_{k,mV}}{\partial r} + \frac{\partial^2 C_{k,mV}}{\partial z^2} \right] = 0$	(58)
Liquid – filled part : $D_{k,mL} \left[\frac{\partial^2 C_{k,mL}}{\partial r^2} + \frac{1}{r} \frac{\partial C_{k,mL}}{\partial r} + \frac{\partial^2 C_{k,mL}}{\partial z^2} \right] + R_{k,mL} = 0$	(59)
$R_{k,mL} = R_k \times \varepsilon$	(60) %
Momentum balance equations:	
Shell-side:	
Radial – direction : $\rho_o \left[v_{r,o} \frac{\partial v_{r,o}}{\partial r} + v_{z,o} \frac{\partial v_{r,o}}{\partial z} \right] = -\frac{\partial P_o}{\partial r} + \mu_o \left\{ \frac{\partial}{\partial r} \left[\frac{1}{r} \frac{\partial}{\partial r} (r v_{r,o}) + \frac{\partial^2 v_{r,o}}{\partial z^2} \right] \right\}$	(61)

Table 7. Cont.

Main Equations	References
Axial – direction : $\rho_o \left[v_{r,o} \frac{\partial v_{z,o}}{\partial r} + v_{z,o} \frac{\partial v_{z,o}}{\partial z} \right] = -\frac{\partial P_o}{\partial z} + \mu_o \left\{ \frac{\partial}{\partial r} \left[\frac{1}{r} \frac{\partial}{\partial r} (rv_{z,o}) + \frac{\partial^2 v_{z,o}}{\partial z^2} \right] \right\}$	(62) [60,84]
Inside HFM: Radial – direction : $\rho_i \left[v_{r,i} \frac{\partial v_{r,i}}{\partial r} + v_{z,i} \frac{\partial v_{r,i}}{\partial z} \right] = -\frac{\partial P_i}{\partial r} + \mu_i \left\{ \frac{\partial}{\partial r} \left[\frac{1}{r} \frac{\partial}{\partial r} (rv_{r,i}) + \frac{\partial^2 v_{r,i}}{\partial z^2} \right] \right\}$	(63) [60,84]
Axial – direction : $\rho_i \left[v_{r,i} \frac{\partial v_{z,i}}{\partial r} + v_{z,i} \frac{\partial v_{z,i}}{\partial z} \right] = -\frac{\partial P_i}{\partial z} + \mu_i \left\{ \frac{\partial}{\partial r} \left[\frac{1}{r} \frac{\partial}{\partial r} (rv_{z,i}) + \frac{\partial^2 v_{z,i}}{\partial z^2} \right] \right\}$	(64) [60,84]
Energy balance equations: Shell-side: $\Omega_o \left[\frac{\partial^2 T_o}{\partial r^2} + \frac{1}{r} \frac{\partial T_o}{\partial r} + \frac{\partial^2 T_o}{\partial z^2} \right] + R_k \Delta H_r = \rho_o C_{P_o} \left(v_{r,o} \frac{\partial T_o}{\partial r} + v_{z,o} \frac{\partial T_o}{\partial z} \right)$	(65) @ [60]
Inside HFM: $\Omega_i \left[\frac{\partial^2 T_i}{\partial r^2} + \frac{1}{r} \frac{\partial T_i}{\partial r} + \frac{\partial^2 T_i}{\partial z^2} \right] + R_k \Delta H_r = \rho_i C_{P_i} \left(v_{r,i} \frac{\partial T_i}{\partial r} + v_{z,i} \frac{\partial T_i}{\partial z} \right)$	(66) # [60]
HFM: $\Omega_m \left[\frac{\partial^2 T_m}{\partial r^2} + \frac{1}{r} \frac{\partial T_m}{\partial r} + \frac{\partial^2 T_m}{\partial z^2} \right] = 0$	(67) [60]

where: k_r : kinetic constant for “k” (m/s); C_{L_j} : L molar concentration of “j” (mol/m³); $D_{k,o}$: diffusivity of “k” in the shell-side (mol/m³); $C_{k,o}$: molar concentration of “k” in the shell-side (mol/m³); $v_{z,o}$: velocity in axial direction in the shell-side (m/s); $v_{r,o}$: velocity in radial direction in the shell-side (m/s); $\bar{v}_{z,o}$: average velocity in axial direction in the shell-side (m/s); d_o : external HFM diameter (m); $D_{k,i}$: diffusivity of “k” inside HFM (mol/m³); $C_{k,i}$: molar concentration of “k” inside HFM (mol/m³); $v_{z,i}$: velocity in axial direction inside HFM (m/s); $v_{r,i}$: Velocity in radial direction inside HFM (m/s); $\bar{v}_{z,i}$: average velocity in axial direction inside HFM (m/s); $D_{k,m}$: Diffusivity of “k” inside membrane pores (mol/m³); $C_{k,m}$: molar concentration of “k” inside membrane pores (mol/m³); $D_{k,mV}$: diffusivity of “k” inside the gas-filled part of HFM pores (mol/m³); $C_{k,mV}$: molar concentration of “k” inside the gas-filled part of HFM pores (mol/m³); $D_{k,mL}$: diffusivity of “k” inside the liquid-filled part of HFM pores (mol/m³); $C_{k,mL}$: molar concentration of “k” inside the liquid-filled part of HFM pores (mol/m³); $R_{k,mL}$: chemical reaction rate of “k” inside the liquid-filled part of HFM pores (mol/(m³.s)); ρ_o : density in the shell-side (kg/m³); ρ_i : density inside HFM (kg/m³); Ω_o : heat transfer coefficient of stream in the shell-side (W/(m².K)); T_o : shell-side temperature (K); C_{P_o} : mass isobaric heat capacities in the shell-side (J/(kg.K)); Ω_i : heat transfer coefficient inside HFM (W/(m².K)); T_i : HFM inside temperature (K); C_{P_i} : mass isobaric heat capacities inside HFM (J/(kg.K)); T_m : HFM temperature (K). @ R_k term only appears in this equation if the solvent flows in the shell-side; # R_k term only appears in this equation if the solvent flows inside the HFM; \$ The diffusivity-term of the equation depends on which side of HFM the gas flows; % In membrane section, chemical reactions occur just inside the pores.

Table 8. 1D-2D models not related to processing simulators.

Main Equations	References
<p style="text-align: center;">Mass balance equation:</p> $D_{k,i} \left[\frac{\partial^2 C_{k,i}}{\partial r^2} + \frac{1}{r} \frac{\partial C_{k,i}}{\partial r} \right] - R_{k,i} = v_{z,i} \frac{\partial C_{k,i}}{\partial z} \quad (68)$	[78,169,171]
Velocity distribution: (Newtonian laminar flow) Equation (55)	[78,169,171]

The following works were conducted in the context of post-combustion carbon capture. They are considered in the present review as low-pressure GLMC CO₂ stripping from the solvent is conducted similarly for both GLMC processes for carbon capture from NG and flue gas. Scholes [173] used a simple model and a 1D rigorous model (Table 6, Equations (35)–(37), (39), (40), (42), and (44)–(46)) with mass/energy balances and pressure drop calculation to study vacuum-driven CO₂ stripping from aqueous-MEA 30 w/w%, using steam as stripping-gas. The best stripping temperature was found between 90 °C and 105 °C. Above this temperature range, the solvent starts vaporizing, and below this range, the mass transfer driving force is drastically reduced. Scholes highlighted the trade-off between the reduction of stripping heat requirement against the vacuum pump power requirement. Zaidiza et al. [174] developed a GLMC model for post-combustion CO₂ absorption with aqueous-MEA solvent and for the respective CO₂ stripping. The 1D adiabatic model (Table 6, Equations (35)–(39) and (41)–(46)) considers the bidirectional mass transfer of all species (CO₂, H₂O, MEA); energy balances; and head-loss calculations via Hagen-Poiseuille equation for the HFM stream and via Happel equation [175] for the shell-side. Model equations were presented with dimensional problems and inverted signs (e.g., Pa.s⁻¹ was the viscosity unit instead of Pa.s). Model assumptions include steady-state, ideal gas behavior, and VLE via Henry's law. Water condensation/evaporation was considered at the liquid-membrane interface. The authors emphasize that GLMC-stripper needs HFM resistant to high temperatures (≈120 °C). Also, since water can be transferred in both directions, capillary condensation can occur, which would negatively influence mass transfer performance similarly to MPW.

4.3. GLMC Models Not Related to Process Simulators

The main GLMC models not related to processing simulators are presented in Table 6 for 1D models, Table 7 for 2D models, and Table 8 for 1D-2D models. These models were already discussed in Section 4.1 and are detailed here for completeness. They usually lack thermodynamic frameworks and present several simplifications, such as isothermal GLMC and ideal gas behavior. These tables list equations and modeling strategies adopted, showing that several researchers used the same equations. Table 9 presents the used software for the numerical solution of GLMC equations.

Table 9. Software for solving GLMC models.

Software	References
MATLAB	[33,69,78,135–137,171,173,174]
OpenFOAM	[146]
COMSOL	[60,65,69,76,79,82,84,90,130–134,139,141,143–145,147–150,168,170,172]
PARDISO	[166]
ANSYS	[142]

5. Concluding Remarks and Future Prospects

Aqueous-amine solvents are the most studied in high-pressure NG sweetening and in solvent regeneration with GLMC. Regarding physical solvents, the increasing interest in ionic liquids is highlighted.

Both experimental and modeling GLMC works on carbon capture from CO₂-rich NG must consider all the real offshore operating conditions: (i) high-pressure operation;

(ii) mass transfer of all species, including CO₂, H₂S, CH₄, H₂O, and other light hydrocarbons; (iii) thermal effects, with outlet temperatures assessment; (iv) head-losses of both phases.

Several experimental works were restricted to CO₂ mass transfer at low pressures. The most useful experimental GLMC works so far investigated high-pressure simultaneous CO₂/H₂S removal from gas mixtures containing CH₄, as in [100,101]. Experimental works were usually focused on inlet conditions optimizations to enhance CO₂ mass transfer. To our knowledge, there are no works in the literature providing data on water mass transfer. Pressure drop is frequently neglected in the bench scale but should be investigated at least in the pilot scale. Data of light hydrocarbons (C₂⁺) mass transfer are also scarce. Therefore, future experimental works should perform complete outlet conditions assessments, providing a complete understanding of GLMC behavior.

The development of GLMC models not related to processing simulators is a complex work and imposes an additional task: the supply of a thermodynamic framework for correct RVLE calculation and thermodynamic and transport properties prediction. This was done in de Medeiros et al. [33], in which a full thermodynamic framework was provided for simulation of CO₂ removal from high-pressure NG with a 1D GLMC model considering rigorous multicomponent mass, energy, and momentum balances.

Among the scarce GLMC models that apply at least mass, energy, and momentum balances, Ghasem et al. [60] provided a 2D model for CO₂ absorption from NG, while Scholes [173] and Zaidiza et al. [174] provided 1D models for CO₂ stripping from the solvent. On the other hand, it can be seen in Tables 6–9 that several 2D models are performing CO₂ mass transfer with simplifications such as isothermal condition, ideal gas behavior, and zero pressure drop, using COMSOL or CFD to solve GLMC equations via finite elements. It can be concluded that these models are simplified and cannot reproduce industrial GLMC behavior for NG conditioning with accuracy. Typical examples are [80,150], which proposed 2D models for isothermal CO₂ absorption from NG with aqueous-amine solvents.

GLMC modeling and its implementation in up-to-date process simulators are of great importance to enable industrial-scale technical-economic assessment. In [156,157], mass, energy, and momentum balances were considered, but the multicomponent mass transfer was not. In [161,162], despite considering energy balance and multicomponent mass transfer, the thermodynamic framework is inadequate, and there is no pressure drop calculation. Da Cunha et al. [128] developed a GLMC-UOE to access HYSYS full thermodynamics. Just CO₂ mass transfer was considered, and the model lacks energy and momentum balances. The point here is that to obtain a complete GLMC model to be installed in process simulators, the model must gather all the positive aspects of [128,156,157,161,162].

Moreover, it is worthwhile to think of distributed parameters models as in [33] for GLMC-absorber and [174] for GLMC-stripper. The work of Lock et al. [176] created an MP unit operation extension (MP-UOE) installed in Aspen HYSYS with the same method as da Cunha et al. [128] for GLMC-UOE. To construct the MP-UOE distributed model [176], the succession of states approach was employed, in which the equipment is divided into many finite cells in the axial direction. In the same way, it would be interesting to develop a GLMC complete distributed model to be installed in Aspen HYSYS as GLMC-UOE or in other available process simulators.

Author Contributions: Conceptualization J.L.d.M.; methodology, J.L.d.M. and O.d.Q.F.A.; formal analysis, G.P.d.C., J.L.d.M., and O.d.Q.F.A.; investigation, G.P.d.C. and J.L.d.M.; data curation, G.P.d.C.; writing—original draft preparation, G.P.d.C. and J.L.d.M.; visualization, G.P.d.C.; writing—review and editing, J.L.d.M. and O.d.Q.F.A.; supervision, J.L.d.M. and O.d.Q.F.A.; project administration, J.L.d.M. and O.d.Q.F.A. All authors have read and agreed to the published version of the manuscript.

Funding: J.L.d.M. and O.d.Q.F.A. acknowledge financial support from CNPq-Brazil (313861/2020-0 and 312328/2021-4).

Institutional Review Board Statement: Not applicable.

Informed Consent Statement: Not applicable.

Data Availability Statement: Not applicable.

Conflicts of Interest: The authors declare no conflict of interest.

Abbreviations

1D	One-Dimensional
2D	Two-Dimensional
AGWA	Acid-Gas Water Alkanolamines
CCS	Carbon Capture and Storage
CCUS	Carbon Capture Utilization and Storage
CFD	Computational Fluid Dynamics
ChA	Chemical-Absorption
DEPG	Dimethyl Ether of Polyethylene Glycol
DLL	Dynamic-Link Library
EDF	Extension Definition File
EMWR	Equivalent Moles Without Reaction
e-NRTL	Electrolyte Non-Random Two Liquid
EGR	Enhanced Gas Recovery
EOR	Enhanced Oil Recovery
GHG	Greenhouse Gas
GLMC	Gas-Liquid Membrane Contactor
GLMC-UOE	Gas-Liquid Membrane Contactor HYSYS Unit Operation Extension
HFM	Hollow-Fiber Membrane
MDEA	Methyldiethanolamine
MEA	Monoethanolamine
MMNm ³ /d	Millions of Normal Cubic Meters per Day
MP	Membrane Permeation
MP-UOE	MP-UOE Membrane Permeation Unit Operation Extension
MPW	Membrane Pore Wetting
NG	Natural Gas
NRM	Newton-Raphson Method
ODE	Ordinary Differential Equations
PC-SAFT	Perturbed Chain Statistical Association Fluid Theory Equation-of-State
PFD	Process Flow Diagram
PMP	Partial Molar Property
PP	Polypropylene
PPO	Polyphenylene Oxide
PR	Peng-Robinson Equation-of-State
PSA	Pressure Swing Adsorption
RVLE	Reactive Vapor-Liquid Equilibrium
UOE	Unit Operation Extension
VLE	Vapor-Liquid Equilibrium
WDPA	Water Dew-Point Adjustment

Nomenclature

A_{SISA}	Specific inner surface area of GLMC module (m^2/m^3)
A_E, A_I	External/internal convective heat exchange areas (m^2)
A_{CSHF}	Cross-section area inside HFM (m^2)
A_{CSS}	Cross-section area within GLMC shell and outside HFM (m^2)
a_{ext}	External specific interfacial area (-)

a_{int}	Internal specific interfacial area (-)
a_m	Specific membrane area (-)
A	Mass transfer area of the GLMC battery (m^2)
$C_{V,k}, C_{L,k}$	Molar concentration of "k" in V stream and L stream (mol/m^3)
$C_{k,i}$	Molar concentration of "k" inside HFM (mol/m^3)
$C_{k,m}$	Molar concentration of "k" inside membrane pores (mol/m^3)
$C_{k,mL}$	Molar concentration of "k" inside the liquid-filled part of HFM pores (mol/m^3)
$C_{k,mV}$	Molar concentration of "k" inside the gas-filled part of HFM pores (mol/m^3)
$C_{k,o}$	Molar concentration of "k" in the shell side (mol/m^3)
$C_{L,j}$	Molar concentration of "j" in L (mol/m^3)
$C_{L,k}^*$	Molar concentration of "k" in L at equilibrium (mol/m^3)
$C_{L,k,m}$	Concentration of "k" at liquid-membrane interface (mol/m^3)
\bar{C}_{V,CO_2}	Average V concentration of CO_2 (mol/m^3)
$\bar{C}_{P_V}, \bar{C}_{P_L}$	V and L molar isobaric heat capacities ($kJ/(kmol.K)$)
$\bar{C}_{P_{V,k}}$	V partial molar isobaric heat capacities of species "k" ($kJ/(kmol.K)$)
C_{P_i}	Mass isobaric heat capacities of stream inside HFM ($J/(kg.K)$)
C_{P_o}	Mass isobaric heat capacities in the shell side ($J/(kg.K)$)
C_{P_V}, C_{P_L}	V and L mass isobaric heat capacities ($J/(kg.K)$)
D	GLMC shell internal diameter (m)
$D_{CO_2,V}$	V CO_2 diffusivity (m^2/s)
$D_{k,m}^{eff}$	Effective membrane diffusivity of "k" (m^2/s)
D_k	Molecular diffusivity of "k" (m^2/s)
$D_{k,L}$	L diffusivity of "k" (m^2/s)
D_{Kn}	Knudsen diffusivity (m^2/s)
D_m	Membrane diffusivity (m^2/s)
$D_{m,L}$	Diffusivity of membrane at liquid phase (m^2/s)
D_p	Combined diffusivity (m^2/s)
$D_{k,i}$	Diffusivity of "k" inside HFM (mol/m^3)
$D_{k,m}$	Diffusivity of "k" inside membrane pores (mol/m^3)
$D_{k,mL}$	Diffusivity of "k" inside the liquid-filled part of HFM pores (mol/m^3)
$D_{k,mV}$	Diffusivity of "k" inside the gas-filled part of HFM pores (mol/m^3)
$D_{k,o}$	Diffusivity of "k" in the shell-side (mol/m^3)
d_i, d_o	Internal/external HFM diameter (m)
E	Enhancement factor
$E_{V,k}, E_{L,k}^{EMWR}$	PMP ^{EMWR} energies of "k" in V and L (kJ/mol)
F_L	L volumetric flowrate (m^3/s)
$\hat{f}_{L,k}^{in}, \hat{f}_{L,k}^{out}$	Vector of L inlet/outlet fugacities of "k" (bar)
$\hat{f}_{V,k}, \hat{f}_{L,k}$	V and L fugacities of real species "k" (bar)
g	Gravity acceleration ($9.81 m/s^2$)
$\Delta H_{k,abs/evap}$	Enthalpy of absorption or vaporization ($kJ/kmol$);
ΔH_r	Enthalpy of reaction ($kJ/kmol$)
$k_{k,V}$	Gas film mass transfer coefficient of "k" ($mol/(m^2.s.kPa)$)
$k_{k,L}$	Liquid film mass transfer coefficient of "k" ($mol/(m^2.s.kPa)$)
$k_{k,m}$	Membrane mass transfer coefficient of "k" ($mol/(m^2.s.kPa)$)
$k_{k,ov}$	Overall mass transfer coefficient of "k" (m/s)
K_{koz}	Kozeny factor (m^{-2})
k_r	Kinetic constant for "k" (m/s)
L_k^{flux}	L stream molar flux of "k" (mol/s)
L_k	L molar flowrate of "k" (mol/s)
M_V, M_L	V and L EMWR molar masses (kg/mol)
$M_{V,k}, M_{L,k}$	V and L molar masses of "k" (kg/mol)
N_{HF}	Number of HFM within GLMC module
N_k^{flux}	Trans-membrane fluxes of real species "k" ($mol/(s.m^2)$)
N_k	Trans-membrane mass transfer rates of "k" (mol/s)

N_M	Number of GLMC modules
n_{RS}	Number of real species
P_k^{sat}	Saturation pressure of “k” (bar)
P_i	Pressure inside HFM (bar)
P_o	Pressure in the shell-side (bar)
P_V, P_L	V and L absolute pressures (bar)
P_{V_k}	Partial pressure of “k” (bar)
q_V, q_L, q	V and L mass flowrates (kg/s); HFM mass flux (kg/(s.m ²))
q_{V_k}, q_{L_k}	V and L mass flowrates of “k” (kg/s)
Q^{flux}	Heat flux (W/m ²)
Q	Heat rate (kJ/h)
R	Ideal gas constant (8.314 J/(mol.K))
R_k	Chemical reaction rate in terms of “k” (mol/(m ³ .s))
$R_{k,mL}$	Chemical reaction rate of “k” inside the liquid-filled part of HFM pores (mol/(m ³ .s))
r	GLMC radial position (m)
r_i, r_o	Internal/external HFM radius (m)
r_{shell}	Outer radius of virtual cylindrical domain around each HFM (effective radius of shell-side) (m)
r_i^+	Gas-membrane interface at the pore-side (m)
$Sa = N_{HF} \Pi d_o$	Interfacial area per length (m)
S_V, S_L	Sections of V and L flows (m ²)
T^{amb}	Outside temperature (K)
T, T_V, T_L	Temperature, V and L temperatures (K)
$T_{L,m}$	Temperature at liquid–membrane interface (K)
T_i	HFM inside temperature (K)
T_m	HFM temperature (K)
T_o	Shell-side temperature (K)
U	Overall heat transfer coefficient (kJ/(h.m ² .K)) or (W/(m ² .K))
V_k^{flux}	V molar flow (flux) of “k” (mol/s)
V_k	V molar flowrate of “k” (mol/s)
v_i, v_o	Interstitial velocity of the stream at internal/external surface of HFM (m/s)
v_V, v_L	V and L flow velocities (m/s)
\bar{v}_V, \bar{v}_L	V and L flow average velocities (m/s)
$v_{r,i}$	Velocity in radial direction inside HFM (m/s)
$v_{r,o}$	Velocity in radial direction in the shell-side (m/s)
$\bar{v}_{z,i}$	Average velocity in axial direction inside HFM (m/s)
$v_{z,i}$	Velocity in axial direction inside HFM (m/s)
$\bar{v}_{z,o}$	Average velocity in axial direction in the shell-side (m/s)
$v_{z,o}$	Velocity in axial direction in the shell-side (m/s)
X_L	Partial liquid penetration
Y_k, X_k	V and L mol fractions of “k”
Z	Compressibility factor
z	GLMC axial position (m)
Greek Symbols	
$\Gamma_{P_V}, \Gamma_{P_L}$	Isothermal compressibility of V and L at RVLE (kg/(Pa.m ³))
$\Gamma_{T_V}, \Gamma_{T_L}$	Isobaric expansivity of V and L at RVLE (kg/(K.m ³))
$\Gamma_{V_k}, \Gamma_{L_k}$	Species “k” mol expansivity of V and L at RVLE ((kg.s)/(mol.m ³))
ε	Membrane porosity
ε_V	Fraction of total area available for gas flow
H_k	Henry’s law constant of “k” ((kPa.m ³)/mol)
θ	GLMC inclination (rad)
λ_V, λ_L	V and L thermal conductivities (W/(m.K))
μ_i	Dynamic viscosity of the predominant phase inside HFM (Pa.s)
μ_o	Dynamic viscosity of the predominant phase in shell-side (Pa.s)
ϕ	Fiber volume fraction (packing ratio) (-)
Π_k	Trans-membrane mass transfer coefficient of “k” (mol/(s.bar.m ²))
ρ_V, ρ_L	V and L densities (kg/m ³)

ρ_i	Density inside HFM (kg/m^3)
ρ_o	Density in the shell-side (kg/m^3)
τ	Membrane tortuosity
ψ_V, ψ_L	Shear stress on contact surfaces in V and L flows (Pa)
Ω_E, Ω_I	External/internal heat transfer coefficients ($\text{kJ}/(\text{h}\cdot\text{m}^2\cdot\text{K})$) or ($\text{W}/(\text{m}^2\cdot\text{K})$)
Ω_V, Ω_L	V and L heat transfer coefficient ($\text{kJ}/(\text{h}\cdot\text{m}^2\cdot\text{K})$) or ($\text{W}/(\text{m}^2\cdot\text{K})$)
Ω_m	HFM heat transfer coefficient ($\text{kJ}/(\text{h}\cdot\text{m}^2\cdot\text{K})$) or ($\text{W}/(\text{m}^2\cdot\text{K})$)
Ω_i	Heat transfer coefficient inside HFM ($\text{W}/(\text{m}^2\cdot\text{K})$)
Ω_o	Heat transfer coefficient in the shell-side ($\text{W}/(\text{m}^2\cdot\text{K})$)
Superscripts	
out	at outlet
in	at inlet

References

- Sedej, O.; Mbonimpa, E. CFD Modeling of a Lab-Scale Microwave Plasma Reactor for Waste-to-Energy Applications: A Review. *Gases* **2021**, *1*, 11. [\[CrossRef\]](#)
- Günther, M.; Nissen, V. Effects of the Henry Hub Price on U.S. LNG exports and on gas flows in Western Europe. *Gases* **2021**, *1*, 6. [\[CrossRef\]](#)
- Chandrasekar, A.; Syron, E. Evaluation of Heat Decarbonation Strategies and Their Impact on the Irish Gas Network. *Gases* **2021**, *1*, 14. [\[CrossRef\]](#)
- Shahid, M.Z.; Maulud, A.S.; Bustam, M.A.; Suleman, H.; Halim, H.N.A.; Shariff, A.M. Packed column modelling and experimental evaluation for CO₂ absorption using MDEA solution at high pressure and high CO₂ concentrations. *J. Nat. Gas Sci. Eng.* **2021**, *88*, 103829. [\[CrossRef\]](#)
- Mokhtab, S.; Poe, W.A.; Mak, J.Y. *Handbook of Natural Gas Transmission and Processing—Principles and Practices*, 3rd ed.; Gulf Professional Publishing-Elsevier: Waltham, MA, USA, 2015; pp. 2–125.
- Araújo, O.Q.F.; Reis, A.C.; de Medeiros, J.L.; do Nascimento, J.F.; Grava, W.M.; Musse, A.P.S. Comparative analysis of separation technologies for processing carbon dioxide rich natural gas in ultra-deepwater oil fields. *J. Clean. Prod.* **2017**, *155*, 12–22. [\[CrossRef\]](#)
- Rakhiemah, A.N.; Xu, Y. Economic viability of full-chain CCUS-EOR in Indonesia. *Resour. Conserv. Recycl.* **2022**, *179*, 106069. [\[CrossRef\]](#)
- Amarasinghe, W.; Farzaneh, S.; Fjelde, I.; Sohrabi, M.; Guo, Y. A visual investigation of CO₂ convective mixing in water and oil at the pore scale using a micromodel apparatus at reservoir conditions. *Gases* **2021**, *1*, 5. [\[CrossRef\]](#)
- Liu, S.; Yuan, L.; Liu, W.; Zhao, C.; Zhang, Y.; Song, Y. Study on the influence of various factors on dispersion during enhance natural gas recovery with CO₂ sequestration in depleted gas reservoir. *J. Nat. Gas Sci. Eng.* **2022**, *103*, 104644. [\[CrossRef\]](#)
- Egging-Bratseth, R. A techno-economic perspective on natural gas and its value chain. *Gases* **2021**, *1*, 1. [\[CrossRef\]](#)
- Shi, M.; Xiong, W.; Zhang, X.; Ji, J.; Hu, X.; Tu, Z.; Wu, Y. Highly efficient and selective H₂S capture by task-specific deep eutectic solvents through chemical dual-site absorption. *Sep. Purif. Technol.* **2022**, *283*, 120167. [\[CrossRef\]](#)
- Trueba, L., Jr.; Gaston, T.; Brackin, J.; Miller, J.; You, B.H. Effective strategies to reduce triethylene glycol consumption in natural gas processing plants. *Case Stud. Chem. Environ. Eng.* **2022**, *5*, 100196. [\[CrossRef\]](#)
- Shamsi, M.; Farokhi, S.; Pourghafari, M.; Bayat, A. Tuning the natural gas dew point by Joule-Thomson and Mechanical Refrigeration processes: A comparative energy and exergy analysis. *J. Petrol. Sci. Eng.* **2022**, *212*, 110270. [\[CrossRef\]](#)
- Ecker, A.M.; Klein, H.; Peschel, A. Systematic and efficient optimization-based design of a process for CO₂ removal from natural gas. *Chem. Eng. J.* **2022**, *445*, 136178. [\[CrossRef\]](#)
- Abd, A.A.; Othman, M.R. Biogas upgrading to fuel grade methane using pressure swing adsorption: Parametric sensitivity analysis on an industrial scale. *Fuel* **2022**, *308*, 121986. [\[CrossRef\]](#)
- Abdullah, A.; Idris, I.; Shamsudin, I.K.; Othman, M.R. Methane enrichment from high carbon dioxide content natural gas by pressure swing adsorption. *J. Nat. Gas Sci. Eng.* **2019**, *69*, 102929. [\[CrossRef\]](#)
- Rebello, C.M.; Martins, M.A.F.; Rodrigues, A.E.; Loureiro, J.M.; Ribeiro, A.M.; Nogueira, I.B.R. A novel standpoint of Pressure Swing Adsorption processes multi-objective optimization: An approach based on feasible operation region mapping. *Chem. Eng. Res. Des.* **2022**, *178*, 590–601. [\[CrossRef\]](#)
- Park, K.H.; Lee, J.W.; Lim, Y.; Seo, Y. Life cycle cost analysis of CO₂ compression processes coupled with a cryogenic distillation unit for purifying high-CO₂ natural gas. *J. CO₂ Util.* **2022**, *60*, 102002. [\[CrossRef\]](#)
- Baccanelli, M.; Langé, S.; Rocco, M.V.; Pellegrini, L.A.; Colombo, E. Low temperature techniques for natural gas purification and LNG production: An energy and exergy analysis. *Appl. Energy* **2016**, *180*, 546–559. [\[CrossRef\]](#)
- Shafiq, U.; Shariff, A.M.; Babar, M.; Azeem, B.; Ali, A.; Bustam, A. Study of dry ice formation during blowdown of CO₂-CH₄ from cryogenic distillation column. *J. Loss Prev. Proc.* **2020**, *64*, 104073. [\[CrossRef\]](#)
- Arinelli, L.O.; de Medeiros, J.L.; de Melo, D.C.; Teixeira, A.M.; Brigagão, G.V.; Passarelli, F.M.; Grava, W.M.; Araújo, O.Q.F. Carbon capture and high-capacity supercritical fluid processing with supersonic separator: Natural gas with ultra-high CO₂ content. *J. Nat. Gas Sci. Eng.* **2019**, *66*, 265–283. [\[CrossRef\]](#)

22. Baker, R.W.; Lokhandwala, K. Natural Gas Processing with Membranes: An Overview. *Ind. Eng. Chem. Res.* **2008**, *47*, 2109–2121. [[CrossRef](#)]
23. Law, L.C.; Ng, J.J.Y.; Hasan, M.M.; Othman, M.R.; Helwani, Z.; Idroes, R. Effects of membrane selectivity and configuration on methane purity and recovery from high carbon dioxide content natural gas. *J. Nat. Gas Sci. Eng.* **2021**, *89*, 103882. [[CrossRef](#)]
24. Siagian, U.W.R.; Raksajati, A.; Himma, N.F.; Khoiruddin, K.; Wenten, I.G. Membrane-based carbon capture technologies: Membrane gas separation vs. membrane contactor. *J. Nat. Gas Sci. Eng.* **2019**, *67*, 172–195. [[CrossRef](#)]
25. Shokrollahi, F.; Lau, K.K.; Partoon, B.; Smith, A.M. A review on the selection criteria for slow and medium kinetic solvents used in CO₂ absorption for natural gas purification. *J. Nat. Gas Sci. Eng.* **2022**, *98*, 104390. [[CrossRef](#)]
26. Tan, L.S.; Shariff, A.M.; Lau, K.K.; Bustam, M.A. Impact of high pressure on high concentration carbon dioxide capture from natural gas by monoethanolamine/N-methyl-2-pyrrolidone solvent in absorption packed column. *Int. J. Greenh. Gas Control* **2015**, *34*, 25–30. [[CrossRef](#)]
27. Araújo, O.Q.F.; de Medeiros, J.L. Carbon capture and storage technologies: Present scenario and drivers of innovation. *Curr. Opin. Chem. Eng.* **2017**, *17*, 22–34. [[CrossRef](#)]
28. Kazmi, B.; Raza, F.; Taqvi, S.A.A.; Awan, Z.U.H.; Ali, S.I.; Suleman, H. Energy, exergy and economic (3E) evaluation of CO₂ capture from natural gas using pyridinium functionalized ionic liquids: A simulation study. *J. Nat. Gas Sci. Eng.* **2021**, *90*, 103951. [[CrossRef](#)]
29. Tay, W.H.; Lau, K.K.; Lai, L.S.; Shariff, A.M.; Wang, T. Current development and challenges in the intensified absorption technology for natural gas purification at offshore condition. *J. Nat. Gas Sci. Eng.* **2019**, *71*, 102977. [[CrossRef](#)]
30. Mansourizadeh, A.; Rezaei, I.; Lau, W.J.; Seah, M.Q.; Ismail, A.F. A review on recent progress in environmental applications of membrane contactor technology. *J. Environ. Chem. Eng.* **2022**, *10*, 107631. [[CrossRef](#)]
31. Sabzekar, M.; Chenar, M.P.; Khayet, M.; García-Payo, C.; Maghsoud, Z.; Pagliero, M. Cyclic olefin polymer membrane as an emerging material for CO₂ capture in gas-liquid membrane contactor. *J. Environ. Chem. Eng.* **2022**, *10*, 107669. [[CrossRef](#)]
32. Amaral, R.A.; Habert, C.A.; Borges, C.P. Performance evaluation of composite and microporous gas-liquid membrane contactors for CO₂ removal from a gas mixture. *Chem. Eng. Process. Process Intensif.* **2016**, *102*, 202–209. [[CrossRef](#)]
33. de Medeiros, J.L.; Nakao, A.; Grava, W.M.; Nascimento, J.F.; Araújo, O.Q.F. Simulation of an Offshore Natural Gas Purification Process for CO₂ Removal with Gas-Liquid Contactors Employing Aqueous Solutions of Ethanolamines. *Ind. Eng. Chem. Res.* **2013**, *52*, 7074–7089. [[CrossRef](#)]
34. Kim, S.; Scholes, C.A.; Heath, D.E.; Kentish, S.E. Gas-liquid membrane contactors for carbon dioxide separation: A review. *Chem. Eng. J.* **2021**, *411*, 128468. [[CrossRef](#)]
35. Li, L.; Ma, G.; Pan, Z.; Zhang, N.; Zhang, Z. Research Progress in Gas Separation Using Hollow Fiber Membrane Contactors. *Membranes* **2020**, *10*, 380. [[CrossRef](#)] [[PubMed](#)]
36. Xu, Y.; Goh, K.; Wang, R.; Bae, T.H. A review on polymer-based membranes for gas-liquid membrane contacting processes: Current challenges and future direction. *Sep. Purif. Technol.* **2019**, *229*, 115791. [[CrossRef](#)]
37. Babin, A.; Bougie, F.; Rodrigue, D.; Iliuta, M.C. A closer look on the development and commercialization of membrane contactors for mass transfer and separation processes. *Sep. Purif. Technol.* **2019**, *227*, 115679. [[CrossRef](#)]
38. Ibrahim, M.H.; El-Naas, M.H.; Zhang, Z.; Van der Bruggen, B. CO₂ Capture Using Hollow Fiber Membranes: A Review of Membrane Wetting. *Energy Fuels* **2018**, *32*, 963–978. [[CrossRef](#)]
39. Zhang, Y.; Wang, R. Gas-liquid membrane contactors for acid gas removal: Recent advances and future challenges. *Curr. Opin. Chem. Eng.* **2013**, *2*, 255–262. [[CrossRef](#)]
40. Rivero, J.R.; Panagakos, G.; Lieber, A.; Hornbostel, K. Hollow Fiber Membrane Contactors for Post-Combustion Carbon Capture: A Review of Modeling Approaches. *Membranes* **2020**, *10*, 382. [[CrossRef](#)]
41. Zhao, S.; Feron, P.H.M.; Deng, L.; Favre, E.; Chabanon, E.; Yan, S.; Hou, J.; Chen, V.; Qi, H. Status and progress of membrane contactors in post-combustion carbon capture: A state-of-the-art review of new developments. *J. Membr. Sci.* **2016**, *511*, 180–206. [[CrossRef](#)]
42. Vadillo, J.M.; Gómez-Coma, L.; Garea, A.; Irabien, A. Hollow Fiber Membrane Contactors in CO₂ Desorption: A Review. *Energy Fuels* **2021**, *35*, 111–136. [[CrossRef](#)]
43. Zhang, Z.E.; Yan, Y.F.; Zhang, L.; Ju, S.X. Hollow fiber membrane contactor absorption of CO₂ from the flue gas: Review and perspective. *Glob. Nest J.* **2014**, *16*, 354–373. [[CrossRef](#)]
44. Cui, Z.; de Montigny, D. Part 7: A review of CO₂ capture using hollow fiber membrane contactors. *Carbon Manag.* **2014**, *4*, 69–89. [[CrossRef](#)]
45. Li, J.L.; Chen, B.H. Review of CO₂ absorption using chemical solvents in hollow fiber membrane contactors. *Sep. Purif. Technol.* **2005**, *41*, 109–122. [[CrossRef](#)]
46. Ng, E.L.H.; Lau, K.K.; Lau, W.J.; Ahmad, F. Holistic review on the recent development in mathematical modelling and process simulation of hollow fiber membrane contactor for gas separation process. *J. Ind. Eng. Chem.* **2021**, *104*, 231–257. [[CrossRef](#)]
47. Dalane, K.; Dai, Z.; Mogseth, G.; Hillestad, M.; Deng, L. Potential applications of membrane separation for subsea natural gas processing: A review. *J. Nat. Gas Sci. Eng.* **2017**, *39*, 101–117. [[CrossRef](#)]
48. Bazhenov, S.D.; Bilydukevich, A.V.; Volkov, A.V. Gas-Liquid Hollow Fiber Membrane Contactors for Different Applications. *Fibers* **2018**, *6*, 76. [[CrossRef](#)]

49. Karadas, F.; Atilhan, M.; Aparicio, S. Review on the Use of Ionic Liquids (ILs) as Alternative Fluids for CO₂ Capture and Natural Gas Sweetening. *Energy Fuels* **2010**, *24*, 5817–5828. [[CrossRef](#)]
50. Mansourizadeh, A.; Ismail, A.F. Hollow fiber gas-liquid membrane contactors for acid gas capture: A review. *J. Hazard. Mater.* **2009**, *171*, 38–53. [[CrossRef](#)]
51. Gabelman, A.; Hwang, S.T. Hollow fiber membrane contactors. *J. Membr. Sci.* **1999**, *159*, 61–106. [[CrossRef](#)]
52. Zhang, H.; Xue, K.; Cheng, C.; Gao, D.; Chen, H. Study on the performance of CO₂ capture from flue gas with ceramic membrane contactor. *Sep. Purif. Technol.* **2021**, *265*, 118521. [[CrossRef](#)]
53. Rahbari-Sisakht, M.; Rana, D.; Matsuura, T.; Emadzadeh, D.; Padaki, M.; Ismail, A.F. Study on CO₂ stripping from water through novel surface modified PVDF hollow fiber membrane contactor. *Chem. Eng. J.* **2014**, *246*, 306–310. [[CrossRef](#)]
54. Scholes, C.A.; Kentish, S.E.; Qader, A. Membrane gas-solvent contactor pilot plant trials for post-combustion CO₂ capture. *Sep. Purif. Technol.* **2020**, *237*, 116470. [[CrossRef](#)]
55. Zhang, H.Y.; Wang, R.; Liang, D.T.; Tay, J.H. Modeling and experimental study of CO₂ absorption in a hollow fiber membrane contactor. *J. Membr. Sci.* **2006**, *279*, 301–310. [[CrossRef](#)]
56. Al-Saffar, H.B.; Ozturk, B.; Hughes, R. A comparison of porous and non-porous gas-liquid membrane contactors for gas separation. *Chem. Eng. Res. Des.* **1997**, *75*, 685–692. [[CrossRef](#)]
57. Cesari, L.; Castel, C.; Favre, E. Membrane contactors for intensified gas-liquid absorption processes with physical solvents: A critical parametric study. *J. Membr. Sci.* **2021**, *635*, 119377. [[CrossRef](#)]
58. Reed, B.W.; Semmens, M.J.; Cussler, E.L. Membrane contactors. In *Membrane Separations Technology: Principles and Applications*; Noble, R.D., Stern, S.A., Eds.; Elsevier Science B.V.: New York, NY, USA, 1995; Volume 2, pp. 467–498.
59. Tantikhajongosol, P.; Laosiripojana, N.; Jiraratananon, R.; Assabumrungrat, S. Physical absorption of CO₂ and H₂S from synthetic biogas at elevated pressures. using hollow fiber membrane contactors: The effects of Henry's constants and gas diffusivities. *Int. J. Heat Mass Transf.* **2019**, *128*, 1136–1148. [[CrossRef](#)]
60. Ghasem, N.; Al-Marzouqi, M.; Rahim, N.A. Modeling of CO₂ absorption in a membrane contactor considering solvent evaporation. *Sep. Purif. Technol.* **2013**, *110*, 1–10. [[CrossRef](#)]
61. Keshavarz, P.; Fathikalajahi, J.; Ayatollahi, S. Analysis of CO₂ separation and simulation of a partially wetted hollow fiber membrane contactor. *J. Hazard. Mater.* **2008**, *152*, 1237–1247. [[CrossRef](#)]
62. Nguyen, P.T.; Lasseguette, E.; Medina-Gonzalez, Y.; Remigy, J.C.; Roizard, D.; Favre, E. A dense membrane contactor for intensified CO₂ gas/liquid absorption in post-combustion capture. *J. Membr. Sci.* **2011**, *377*, 261–272. [[CrossRef](#)]
63. Karoor, S.; Sirkar, K.K. Gas Absorption Studies in Microporous Hollow Fiber Membrane Modules. *Ind. Eng. Chem. Res.* **1993**, *32*, 674–684. [[CrossRef](#)]
64. Chen, W.H.; Chen, S.M.; Hung, C.I. Carbon dioxide capture by single droplet using Selexol, Rectisol and water as absorbents: A theoretical approach. *Appl. Energy* **2013**, *111*, 731–741. [[CrossRef](#)]
65. Al-Marzouqi, M.H.; El-Naas, M.H.; Marzouk, S.A.M.; Al-Zarooni, M.A.; Abdullatif, N.; Faiz, R. Modeling of CO₂ absorption in membrane contactors. *Sep. Purif. Technol.* **2008**, *59*, 286–293. [[CrossRef](#)]
66. Xiang, L.; Wu, L.; Gao, L.; Chen, J.; Liu, Y.; Zhao, H. Pilot scale applied research on CO₂ removal of natural gas using a rotating packed bed with propylene carbonate. *Chem. Eng. Res. Des.* **2019**, *150*, 33–39. [[CrossRef](#)]
67. Roussanaly, S.; Anantharaman, R.; Lindqvist, K. Multi-criteria analyses of two solvent and one low-temperature concepts for acid gas removal from natural gas. *J. Nat. Gas Sci. Eng.* **2014**, *20*, 38–49. [[CrossRef](#)]
68. Hughes, T.J.; Kandil, M.E.; Graham, B.F.; May, E.F. Simulating the capture of CO₂ from natural gas: New data and improved models for methane + carbon dioxide + methanol. *Int. J. Greenh. Gas Control* **2014**, *31*, 121–127. [[CrossRef](#)]
69. Sohaib, Q.; Vadillo, J.M.; Gómez-Coma, L.; Albo, J.; Druon-Bocquet, S.; Irabien, A.; Sanchez-Marcano, J. CO₂ capture with room temperature ionic liquids; coupled absorption/desorption and single module absorption in membrane contactor. *Chem. Eng. Sci.* **2020**, *223*, 115719. [[CrossRef](#)]
70. Swati, I.K.; Sohaib, Q.; Khan, H.; Younas, M.; Monjezi, A.H.; Li, J.; Rezakazemi, M. Non-dispersive solvent absorption of post-combustion CO₂ in membrane contactors using ionic liquids. *J. Mol. Liq.* **2022**, *351*, 118566. [[CrossRef](#)]
71. Mandal, B.; Bandyopadhyay, S.S. Simultaneous Absorption of CO₂ and H₂S Into Aqueous Blends of N-Methyldiethanolamine and Diethanolamine. *Environ. Sci. Technol.* **2006**, *40*, 6076–6084. [[CrossRef](#)]
72. Cleeton, C.; Kvam, O.; Rea, R.; Sarkisov, L.; De Angelis, M.G. Competitive H₂S–CO₂ absorption in reactive aqueous methyldiethanolamine solution: Prediction with ePC-SAFT. *Fluid Phase Equilibria* **2020**, *511*, 112453. [[CrossRef](#)]
73. Khan, S.N.; Hailegiorgis, S.M.; Man, Z.; Shariff, A.M.; Garg, S. Thermophysical properties of concentrated aqueous solution of N-methyldiethanolamine (MDEA), piperazine (PZ), and ionic liquids hybrid solvent for CO₂ capture. *J. Mol. Liq.* **2017**, *229*, 221–229. [[CrossRef](#)]
74. Lepaumier, H.; Picq, D.; Carrette, P.L. New Amines for CO₂ Capture. I. Mechanisms of Amine Degradation in the Presence of CO₂. *Ind. Eng. Chem. Res.* **2009**, *48*, 9061–9067. [[CrossRef](#)]
75. Kiani, S.; Taghizade, A.; Ramezani, R.; Di Felice, R.; Molelekwa, G.F.; Mazinani, S. Enhancement of CO₂ removal by promoted MDEA solution in a hollow fiber membrane contactor: A numerical and experimental study. *Carbon Capture Sci. Technol.* **2022**, *2*, 100028. [[CrossRef](#)]
76. Faiz, R.; Al-Marzouqi, M. Mathematical modeling for the simultaneous absorption of CO₂ and H₂S using MEA in hollow fiber membrane contactors. *J. Membr. Sci.* **2009**, *342*, 269–278. [[CrossRef](#)]

77. Zahid, U.; Al Rowaili, F.N.; Ayodeji, M.K.; Ahmed, U. Simulation and parametric analysis of CO₂ capture from natural gas using diglycolamine. *Int. J. Greenh. Gas Control* **2017**, *57*, 42–51. [[CrossRef](#)]
78. Keshavarz, P.; Fathikalajahi, J.; Ayatollahi, S. Mathematical modeling of the simultaneous absorption of carbon dioxide and hydrogen sulfide in a hollow fiber membrane contactor. *Sep. Purif. Technol.* **2008**, *63*, 145–155. [[CrossRef](#)]
79. Razavi, S.M.R.; Shirazian, S.; Najafabadi, M.S. Investigations on the Ability of Di-Isopropanol Amine Solution for Removal of CO₂ From Natural Gas in Porous Polymeric Membranes. *Polym. Eng. Sci.* **2015**, *55*, 598–603. [[CrossRef](#)]
80. Abdolahi-Mansoorkhani, H.; Seddighi, S. CO₂ capture by modified hollow fiber membrane contactor: Numerical study on membrane structure and membrane wettability. *Fuel Process. Technol.* **2020**, *209*, 106530. [[CrossRef](#)]
81. Sutar, P.N.; Jha, A.; Vaidya, P.D.; Kenig, E.Y. Secondary amines for CO₂ capture: A kinetic investigation using N-ethylmonoethanolamine. *Chem. Eng. J.* **2012**, *207–208*, 718–724. [[CrossRef](#)]
82. Rezakazemi, M.; Niazi, Z.; Mirfendereski, M.; Shirazian, S.; Mohammadi, T.; Pak, A. CFD simulation of natural gas sweetening in a gas-liquid hollow-fiber membrane contactor. *Chem. Eng. J.* **2011**, *168*, 1217–1226. [[CrossRef](#)]
83. Boucif, N.; Favre, E.; Roizard, D. CO₂ capture in HFMM contactor with typical amine solutions: A numerical analysis. *Chem. Eng. Sci.* **2008**, *63*, 5375–5385. [[CrossRef](#)]
84. Nakhjiri, A.T.; Heydarinasab, A.; Bakhtiari, O.; Mohammadi, T. Numerical simulation of CO₂/H₂S simultaneous removal from natural gas using potassium carbonate aqueous solution in hollow fiber membrane contactor. *J. Environ. Chem. Eng.* **2020**, *8*, 104130. [[CrossRef](#)]
85. Hatab, F.A.; Abdullatif, N.; Marzouk, S.A.M.; Al-Marzouqi, M.H. Experimental and modeling of CO₂ removal from gas mixture using membrane contactors packed with glass beads. *Sep. Purif. Technol.* **2019**, *217*, 240–246. [[CrossRef](#)]
86. Rahim, N.A.; Ghasem, N.; Al-Marzouqi, M. Absorption of CO₂ from natural gas using different amino acid salt solutions and regeneration using hollow fiber membrane contactors. *J. Nat. Gas Sci. Eng.* **2015**, *26*, 108–117. [[CrossRef](#)]
87. Magnone, E.; Lee, H.J.; Shin, M.C.; Park, J.H. A performance comparison study of five single and sixteen blended amine absorbents for CO₂ capture using ceramic hollow fiber membrane contactors. *J. Ind. Eng. Chem.* **2021**, *100*, 174–185. [[CrossRef](#)]
88. Kang, G.; Chan, Z.P.; Saleh, S.B.M.; Cao, Y. Removal of high concentration CO₂ from natural gas using high pressure membrane contactors. *Int. J. Greenh. Gas Control* **2017**, *60*, 1–9. [[CrossRef](#)]
89. Glasscock, D.A.; Critchfield, J.E.; Rochelle, G.T. CO₂ absorption/desorption in mixture of methyl diethanolamine with monoethanolamine or diethanolamine. *Chem. Eng. Sci.* **1991**, *46*, 2829–2845. [[CrossRef](#)]
90. Mesbah, M.; Momeni, M.; Soroush, E.; Shahsavari, S.; Galledari, S.A. Theoretical study of CO₂ separation from CO₂/CH₄ gaseous mixture using 2-methylpiperazine-promoted potassium carbonate through hollow fiber membrane contactor. *J. Environ. Chem. Eng.* **2019**, *7*, 102781. [[CrossRef](#)]
91. Lu, J.G.; Lu, Z.Y.; Chen, Y.; Wang, J.T.; Gao, L.; Gao, X.; Tang, Y.Q.; Liu, D.G. CO₂ absorption into aqueous blends of ionic liquid and amine in a membrane contactor. *Sep. Purif. Technol.* **2015**, *150*, 278–285. [[CrossRef](#)]
92. Qi, Z.; Cussler, E.L. Microporous hollow fibers for gas absorption: I. Mass transfer in the liquid. *J. Membr. Sci.* **1985**, *23*, 321–332. [[CrossRef](#)]
93. Qi, Z.; Cussler, E.L. Microporous hollow fibers for gas absorption: II. Mass transfer across the membrane. *J. Membr. Sci.* **1985**, *23*, 333–345. [[CrossRef](#)]
94. Dindore, V.Y.; Brilman, D.W.F.; Geuzebroek, F.H.; Versteeg, G.F. Membrane-solvent selection for CO₂ removal using membrane gas-liquid contactors. *Sep. Purif. Technol.* **2004**, *40*, 133–145. [[CrossRef](#)]
95. Atcharyawut, S.; Jiratananon, R.; Wang, R. Separation of CO₂ from CH₄ by using gas-liquid membrane contacting process. *J. Membr. Sci.* **2007**, *304*, 163–172. [[CrossRef](#)]
96. Hedayat, M.; Soltanieh, M.; Mousavi, S.A. Simultaneous separation of H₂S and CO₂ from natural gas by hollow fiber membrane contactor using mixture of alkanolamines. *J. Membr. Sci.* **2011**, *377*, 191–197. [[CrossRef](#)]
97. Al-Marzouqi, M.H.; Marzouk, S.A.M.; El-Naas, M.H.; Abdullatif, N. CO₂ Removal from CO₂-CH₄ Gas Mixture Using Different Solvents and Hollow Fiber Membranes. *Ind. Eng. Chem. Res.* **2009**, *48*, 3600–3605. [[CrossRef](#)]
98. Marzouk, S.A.M.; Al-Marzouqi, M.H.; El-Naas, M.H.; Abdullatif, N.; Ismail, Z.M. Removal of carbon dioxide from pressurized CO₂-CH₄ gas mixture using hollow fiber membrane contactors. *J. Membr. Sci.* **2010**, *351*, 21–27. [[CrossRef](#)]
99. Marzouk, S.A.M.; Al-Marzouqi, M.H.; Abdullatif, N.; Ismail, Z.M. Removal of percentile level of H₂S from pressurized H₂S-CH₄ gas mixture using hollow fiber membrane contactors and absorption solvents. *J. Membr. Sci.* **2010**, *360*, 436–441. [[CrossRef](#)]
100. Marzouk, S.A.M.; Al-Marzouqi, M.H.; Teramoto, M.; Abdullatif, N.; Ismail, Z.M. Simultaneous removal of CO₂ and H₂S from pressurized CO₂-H₂S-CH₄ gas mixture using hollow fiber membrane contactors. *Sep. Purif. Technol.* **2012**, *86*, 88–97. [[CrossRef](#)]
101. Al-Marzouqi, M.H.; Marzouk, S.A.M.; Abdullatif, N. High pressure removal of acid gases using hollow fiber membrane contactors: Further characterization and long-term operational stability. *J. Nat. Gas Sci. Eng.* **2017**, *37*, 192–198. [[CrossRef](#)]
102. Kartohardjono, S.; Paramitha, A.; Putri, A.A.; Andryant, R. Effects of absorbent flow rate on CO₂ absorption through a super hydrophobic hollow fiber membrane contactor. *Int. J. Technol.* **2017**, *8*, 1429–1435. [[CrossRef](#)]
103. Ghobadi, J.; Ramirez, D.; Jerman, R.; Crane, M.; Khoramfar, S. CO₂ separation performance of different diameter polytetrafluoroethylene hollow fiber membranes using gas-liquid membrane contacting system. *J. Membr. Sci.* **2018**, *549*, 75–83. [[CrossRef](#)]
104. Chan, Z.P.; Li, L.; Kang, G.; Manan, N.A.; Cao, Y.; Wang, T. Deep CO₂ removal using high pressure membrane contactors with low liquid-to-gas ratio. *Chem. Eng. Res. Des.* **2020**, *153*, 528–536. [[CrossRef](#)]

105. Petukhov, D.I.; Komkova, M.A.; Eliseev, A.A.; Poyarkov, A.A.; Eliseev, A.A. Nanoporous polypropylene membrane contactors for CO₂ and H₂S capture using alkali absorbents. *Chem. Eng. Res. Des.* **2022**, *177*, 448–460. [[CrossRef](#)]
106. Hosseini, E.; Miandoab, E.S.; Stevens, G.; Scholes, C.A. Vibration-induced enhanced mass transfer within membrane contactors for efficient CO₂ capture. *Sep. Purif. Technol.* **2022**, *295*, 121251. [[CrossRef](#)]
107. Mansourizadeh, A. Experimental study of CO₂ absorption/stripping via PVDF hollow fiber membrane contactor. *Chem. Eng. Res. Des.* **2012**, *90*, 555–562. [[CrossRef](#)]
108. Lu, J.G.; Lu, C.T.; Chen, Y.; Gao, L.; Zhao, X.; Zhang, H.; Xu, Z.W. CO₂ capture by membrane absorption coupling process: Application of ionic liquids. *Appl. Energy* **2014**, *115*, 573–581. [[CrossRef](#)]
109. Mulukutla, T.; Obuskovic, G.; Sirkar, K.K. Novel scrubbing system for post-combustion CO₂ capture and recovery: Experimental studies. *J. Membr. Sci.* **2014**, *471*, 16–26. [[CrossRef](#)]
110. Bazhenov, S.; Malakhov, A.; Bakhtin, D.; Khotimskiy, V.; Bondarenko, G.; Volkov, V.; Ramdin, M.; Vlught, T.J.H.; Volkov, A. CO₂ stripping from ionic liquid at elevated pressure in gas-liquid membrane contactor. *Int. J. Greenh. Gas Control* **2018**, *71*, 293–302. [[CrossRef](#)]
111. Simons, T.J.; Hield, P.; Pas, S.J. A novel experimental apparatus for the study of low temperature regeneration CO₂ capture solvents using hollow fibre membrane contactors. *Int. J. Greenh. Gas Control* **2018**, *78*, 228–235. [[CrossRef](#)]
112. Koonaphadeelert, S.; Wu, Z.; Li, K. Carbon dioxide stripping in ceramic hollow fibre membrane contactors. *Chem. Eng. Sci.* **2009**, *64*, 1–8. [[CrossRef](#)]
113. Khaisri, S.; deMontigny, D.; Tontiwachwuthikul, P.; Jiratananon, R. CO₂ stripping from monoethanolamine using a membrane contactor. *J. Membr. Sci.* **2011**, *376*, 110–118. [[CrossRef](#)]
114. Khaisri, S.; deMontigny, D.; Tontiwachwuthikul, P.; Jiratananon, R. Membrane Contacting Process for CO₂ Desorption. *Energy Procedia* **2011**, *4*, 688–692. [[CrossRef](#)]
115. Scholes, C.A.; Kentish, S.E.; Stevens, G.W.; Jin, J.; deMontigny, D. Thin-film composite membrane contactors for desorption of CO₂ from Monoethanolamine at elevated temperatures. *Sep. Purif. Technol.* **2015**, *156*, 841–847. [[CrossRef](#)]
116. Kianfar, E.; Pirouzfard, V.; Sakhaeinia, H. An experimental study on absorption/stripping CO₂ using mono-ethanol amine hollow fiber membrane contactor. *J. Taiwan Inst. Chem. Eng.* **2017**, *80*, 954–962. [[CrossRef](#)]
117. Lee, H.J.; Kim, M.K.; Park, J.H. Decompression stripping of carbon dioxide from rich monoethanolamine through porous hydrophobic modified ceramic hollow fiber membrane contactor. *Sep. Purif. Technol.* **2020**, *236*, 116304. [[CrossRef](#)]
118. Naim, R.; Ismail, A.F.; Mansourizadeh, A. Preparation of microporous PVDF hollow fiber membrane contactors for CO₂ stripping from diethanolamine solution. *J. Membr. Sci.* **2012**, *392–393*, 29–37. [[CrossRef](#)]
119. Naim, R.; Ismail, A.F.; Mansourizadeh, A. Effect of non-solvent additives on the structure and performance of PVDF hollow fiber membrane contactor for CO₂ stripping. *J. Membr. Sci.* **2012**, *423–424*, 503–513. [[CrossRef](#)]
120. Naim, R.; Ismail, A.F. Effect of polymer concentration on the structure and performance of PEI hollow fiber membrane contactor for CO₂ stripping. *J. Hazard. Mater.* **2013**, *250–251*, 354–361. [[CrossRef](#)]
121. Naim, R.; Ismail, A.F.; Cheer, N.B.; Abdullah, M.S. Polyvinylidene fluoride and polyetherimide hollow fiber membranes for CO₂ stripping in membrane contactor. *Chem. Eng. Res. Des.* **2014**, *92*, 1391–1398. [[CrossRef](#)]
122. Rahbari-Sisakht, M.; Ismail, A.F.; Rana, D.; Matsuura, T. Carbon dioxide stripping from diethanolamine solution through porous surface modified PVDF hollow fiber membrane contactor. *J. Membr. Sci.* **2013**, *427*, 270–275. [[CrossRef](#)]
123. Hosseini, S.; Mansourizadeh, A. Preparation of porous hydrophobic poly(vinylidene fluoride-co-hexafluoropropylene) hollow fiber membrane contactors for CO₂ stripping. *J. Taiwan Inst. Chem. Eng.* **2017**, *76*, 156–166. [[CrossRef](#)]
124. Akan, A.P.; Chau, J.; Sirkar, K.K. Post-combustion CO₂ capture and recovery by pure activated methyl diethanolamine in crossflow membrane contactors having coated hollow fibers. *Sep. Purif. Technol.* **2020**, *244*, 116427. [[CrossRef](#)]
125. Rahim, N.A.; Ghasem, N.; Al-Marzouqi, M. Stripping of CO₂ from different aqueous solvents using PVDF hollow fiber membrane contacting process. *J. Nat. Gas Sci. Eng.* **2014**, *21*, 886–893. [[CrossRef](#)]
126. Wang, Z.; Fang, M.; Pan, Y.; Yan, S.; Luo, Z. Amine-based absorbents selection for CO₂ membrane vacuum regeneration technology by combined absorption-desorption analysis. *Chem. Eng. Sci.* **2013**, *93*, 238–249. [[CrossRef](#)]
127. Kim, S.; Heath, D.E.; Kentish, S.E. Improved carbon dioxide stripping by membrane contactors using hydrophobic electrospun poly(vinylidene fluoride-co-hexafluoropropylene) (PVDF-HFP) membranes. *Chem. Eng. J.* **2022**, *428*, 131247. [[CrossRef](#)]
128. da Cunha, G.P.; de Medeiros, J.L.; Araújo, O.Q.F. Technical Evaluation of the Applicability of Gas-Liquid Membrane Contactors for CO₂ Removal from CO₂ Rich Natural Gas Streams in Offshore Rigs. *Mater. Sci. Forum* **2019**, *965*, 29–38. [[CrossRef](#)]
129. Dindore, V.Y.; Brillman, D.W.F.; Versteeg, G.F. Modelling of cross-flow membrane contactors: Mass transfer with chemical reactions. *J. Membr. Sci.* **2005**, *255*, 275–289. [[CrossRef](#)]
130. Al-Marzouqi, M.; El-Naas, M.; Marzouk, S.; Abdullatif, N. Modeling of chemical absorption of CO₂ in membrane contactors. *Sep. Purif. Technol.* **2008**, *62*, 499–506. [[CrossRef](#)]
131. Faiz, R.; Al-Marzouqi, M. H₂S absorption via carbonate solution in membrane contactors: Effect of species concentrations. *J. Membr. Sci.* **2010**, *350*, 200–210. [[CrossRef](#)]
132. Faiz, R.; Al-Marzouqi, M. CO₂ removal from natural gas at high pressure using membrane contactors: Model validation and membrane parametric studies. *J. Membr. Sci.* **2010**, *365*, 232–241. [[CrossRef](#)]
133. Faiz, R.; Al-Marzouqi, M. Insights on natural gas purification: Simultaneous absorption of CO₂ and H₂S using membrane contactors. *Sep. Purif. Technol.* **2011**, *76*, 351–361. [[CrossRef](#)]

134. Faiz, R.; El-Naas, M.H.; Al-Marzouqi, M. Significance of gas velocity change during the transport of CO₂ through hollow fiber membrane contactors. *Chem. Eng. J.* **2011**, *168*, 593–603. [[CrossRef](#)]
135. Boributh, S.; Assabumrungrat, S.; Laosiripojana, N.; Jiraratananon, R. Effect of membrane module arrangement of gas-liquid membrane contacting process on CO₂ absorption performance: A modeling study. *J. Membr. Sci.* **2011**, *372*, 75–86. [[CrossRef](#)]
136. Boributh, S.; Assabumrungrat, S.; Laosiripojana, N.; Jiraratananon, R. A modeling study on the effects of membrane characteristics and operating parameters on physical absorption of CO₂ by hollow fiber membrane contactor. *J. Membr. Sci.* **2011**, *380*, 21–33. [[CrossRef](#)]
137. Boributh, S.; Rongwong, W.; Assabumrungrat, S.; Laosiripojana, N.; Jiraratananon, R. Mathematical modeling and cascade design of hollow fiber membrane contactor for CO₂ absorption by monoethanolamine. *J. Membr. Sci.* **2012**, *401–402*, 175–189. [[CrossRef](#)]
138. Cai, J.J.; Hawboldt, K.; Abdi, M.A. Contaminant removal from natural gas using dual hollow fiber membrane contactors. *J. Membr. Sci.* **2012**, *397–398*, 9–16. [[CrossRef](#)]
139. Ghasem, N.; Al-Marzouqi, M.; Rahim, N.A. Absorption of CO₂ Form Natural Gas via Gas-Liquid PVDF Hollow Fiber Membrane Contactor and Potassium Glycinate as Solvent. *J. Teknol.* **2014**, *69*, 121–126. [[CrossRef](#)]
140. de Medeiros, J.L.; Barbosa, L.C.; Araújo, O.Q.F. Equilibrium Approach for CO₂ and H₂S Absorption with Aqueous Solutions of Alkanolamines: Theory and Parameter Estimation. *Ind. Eng. Chem. Res.* **2013**, *52*, 9203–9226. [[CrossRef](#)]
141. Faiz, R.; Li, K.; Al-Marzouqi, M. H₂S absorption at high pressure using hollow fibre membrane contactors. *Chem. Eng. Process Process Intensif.* **2014**, *83*, 33–42. [[CrossRef](#)]
142. Cai, J.J.; Hawboldt, K.; Abdi, M.A. Analysis of the effect of module design on gas absorption in cross flow hollow fiber membrane contactors via computational fluid dynamics (CFD) analysis. *J. Membr. Sci.* **2016**, *520*, 415–424. [[CrossRef](#)]
143. Nakhjiri, A.T.; Heydarinasab, A.; Bakhtiari, O.; Mohammadi, T. Experimental investigation and mathematical modeling of CO₂ sequestration from CO₂/CH₄ gaseous mixture using MEA and TEA aqueous absorbents through polypropylene hollow fiber membrane contactor. *J. Membr. Sci.* **2018**, *565*, 1–13. [[CrossRef](#)]
144. Nakhjiri, A.T.; Heydarinasab, A.; Bakhtiari, O.; Mohammadi, T. The effect of membrane porosity wettability on CO₂ removal from CO₂/CH₄ gaseous mixture using NaOH, MEA and TEA liquid absorbents in hollow fiber membrane contactor. *Chin. J. Chem. Eng.* **2018**, *26*, 1845–1861. [[CrossRef](#)]
145. Nakhjiri, A.T.; Heydarinasab, A. Computational simulation and theoretical modeling of CO₂ separation using EDA, PZEA and PS absorbents inside the hollow fiber membrane contactor. *J. Ind. Eng. Chem.* **2019**, *78*, 106–115. [[CrossRef](#)]
146. Fougérit, V.; Pozzobon, V.; Pareau, D.; Théoleyre, M.A.; Stambouli, M. Experimental and numerical investigation binary mixture mass transfer in a gas—Liquid membrane contactor. *J. Membr. Sci.* **2019**, *572*, 1–11. [[CrossRef](#)]
147. Zhang, N.; Pan, Z.; Zhang, L.; Zhang, Z. Decarburization characteristics of coalbed methane by membrane separation technology. *Fuel* **2019**, *242*, 470–478. [[CrossRef](#)]
148. Pan, Z.; Zhang, N.; Zhang, W.; Zhang, Z. Simultaneous removal of CO₂ and H₂S from coalbed methane in a membrane contactor. *J. Clean. Prod.* **2020**, *273*, 123107. [[CrossRef](#)]
149. Ghasem, N. Modeling and Simulation of the Simultaneous Absorption/Stripping of CO₂ with Potassium Glycinate Solution in Membrane Contactor. *Membranes* **2020**, *10*, 72. [[CrossRef](#)]
150. Ghasem, N. Modeling and simulation of the hollow fiber bore size on the CO₂ absorption in membrane contactor. *Chem. Prod. Process Model.* **2020**, *15*, 20190121. [[CrossRef](#)]
151. Kerber, J.; Repke, J.U. Mass transfer and selectivity analysis of a dense membrane contactor for upgrading biogas. *J. Membr. Sci.* **2016**, *520*, 450–464. [[CrossRef](#)]
152. Villeneuve, K.; Zaidiza, D.A.; Roizard, D.; Rode, S. Modeling and simulation of CO₂ capture in aqueous ammonia with hollow fiber composite membrane contactors using a selective dense layer. *Chem. Eng. Sci.* **2018**, *190*, 345–360. [[CrossRef](#)]
153. Villeneuve, K.; Hernandez, A.A.T.; Zaidiza, D.A.; Roizard, D.; Rode, S. Effects of water condensation on hollow fiber membrane contactor performance for CO₂ capture by absorption into a chemical solvent. *J. Membr. Sci.* **2018**, *556*, 365–373. [[CrossRef](#)]
154. Usman, M.; Dai, Z.; Hillestad, M.; Deng, L. Mathematical modeling and validation of CO₂ mass transfer in a membrane contactor using ionic liquids for pre-combustion CO₂ capture. *Chem. Eng. Res. Des.* **2017**, *123*, 377–387. [[CrossRef](#)]
155. Usman, M.; Hillestad, M.; Deng, L. Assessment of a membrane contactor process for pre-combustion CO₂ capture by modelling and integrated process simulation. *Int. J. Greenh. Gas Control* **2018**, *71*, 95–103. [[CrossRef](#)]
156. Hoff, K.A.; Juliussen, O.; Falk-Pedersen, O.; Svendsen, H.F. Modeling and Experimental Study of Carbon Dioxide Absorption in Aqueous Alkanolamine Solutions Using a Membrane Contactor. *Ind. Eng. Chem. Res.* **2004**, *43*, 4908–4921. [[CrossRef](#)]
157. Hoff, K.A.; Svendsen, H.F. CO₂ absorption with membrane contactors vs. packed absorbers—Challenges and opportunities in post combustion capture and natural gas sweetening. *Energy Procedia* **2013**, *37*, 952–960. [[CrossRef](#)]
158. Weiland, R.H.; Chakravarty, T.; Mather, A.E. Solubility of Carbon Dioxide and Hydrogen Sulfide in Aqueous Alkanolamines. *Ind. Eng. Chem. Res.* **1993**, *32*, 1419–1430. [[CrossRef](#)]
159. Kuranov, G.; Rumpf, B.; Maurer, G.; Smirnova, N. VLE modelling for aqueous systems containing methyldiethanolamine, carbon dioxide and hydrogen sulfide. *Fluid Phase Equilibria* **1997**, *136*, 147–162. [[CrossRef](#)]
160. Quek, V.C.; Shah, N.; Chachuat, B. Modeling for design and operation of high-pressure membrane contactors in natural gas sweetening. *Chem. Eng. Res. Des.* **2018**, *132*, 1005–1019. [[CrossRef](#)]
161. Quek, V.C.; Shah, N.; Chachuat, B. Plant-wide assessment of high-pressure membrane contactors in natural gas sweetening—Part I: Model development. *Sep. Purif. Technol.* **2021**, *258*, 117898. [[CrossRef](#)]

162. Quek, V.C.; Shah, N.; Chachuat, B. Plant-wide assessment of high-pressure membrane contactors in natural gas sweetening—Part II: Process analysis. *Sep. Purif. Technol.* **2021**, *258*, 117938. [[CrossRef](#)]
163. Aspen HYSYS®V8 Highlights, Resources, IT Support for V8. AspenTech. aspenONE®Engineering—May 2015. Available online: <https://www.aspentech.com/Aspen-HYSYS-V8-eBook.pdf> (accessed on 21 June 2021).
164. Dymont, J.; Watanasiri, S. Acid Gas Cleaning Using Amine Solvents: Validation with Experimental and Plant Data. AspenTech. White Paper. Aspen Technology Inc. 2018. Available online: <https://www.aspentech.com/en/resources/white-papers/acid-gas-cleaning-using-amine-solvents---validation-with-experimental-and-plant-data> (accessed on 21 June 2021).
165. Arinelli, L.O.; Trotta, T.A.F.; Teixeira, A.M.; de Medeiros, J.L.; Araújo, O.Q.F. Offshore processing of CO₂ rich natural gas with supersonic separator versus conventional routes. *J. Nat. Gas Sci. Eng.* **2017**, *46*, 199–221. [[CrossRef](#)]
166. Mehdipourghazi, M.; Barati, S.; Varaminian, F. Mathematical modeling and simulation of carbon dioxide stripping from water using hollow fiber membrane contactors. *Chem. Eng. Process. Process Intensif.* **2015**, *95*, 159–164. [[CrossRef](#)]
167. Lee, S.; Kim, J.; Lee, E.; Hong, S. Improving the performance of membrane contactors for carbon dioxide stripping from water: Experimental and theoretical analysis. *J. Membr. Sci.* **2022**, *654*, 120552. [[CrossRef](#)]
168. Bahlake, A.; Farivar, F.; Dabir, B. New 3-dimensional CFD modeling of CO₂ and H₂S simultaneous stripping from water within PVDF hollow fiber membrane contactor. *Heat Mass Transf.* **2016**, *52*, 1295–1304. [[CrossRef](#)]
169. Vadillo, J.M.; Gómez-Coma, L.; Garea, A.; Irabien, A. CO₂ Desorption Performance from Imidazolium Ionic Liquids by Membrane Vacuum Regeneration Technology. *Membranes* **2020**, *10*, 234. [[CrossRef](#)]
170. Ghadiri, M.; Marjani, A.; Shirazian, S. Mathematical modeling and simulation of CO₂ stripping from monoethanolamine solution using nano porous membrane contactors. *Int. J. Greenh. Gas Control* **2013**, *13*, 1–8. [[CrossRef](#)]
171. Wang, Z.; Fang, M.; Yu, H.; Ma, Q.; Luo, Z. Modeling of CO₂ Stripping in a Hollow Fiber Membrane Contactor for CO₂ Capture. *Energy Fuels* **2013**, *27*, 6887–6898. [[CrossRef](#)]
172. Mohammed, H.N.; Ahmed, S.M.R.; Al-Naseri, H.; Al-Dahhan, M. Enhancement of CO₂ desorption from MEA-based nanofluids in membrane contactor: Simulation study. *Chem. Eng. Process. Process Intensif.* **2021**, *168*, 108582. [[CrossRef](#)]
173. Scholes, C.A. Membrane contactors modelled for process intensification post combustion solvent regeneration. *Int. J. Greenh. Gas Control* **2019**, *87*, 203–210. [[CrossRef](#)]
174. Zaidiza, D.A.; Belaisaoui, B.; Rode, S.; Favre, E. Intensification potential of hollow fiber membrane contactors for CO₂ chemical absorption and stripping using monoethanolamine solutions. *Sep. Purif. Technol.* **2017**, *188*, 38–51. [[CrossRef](#)]
175. Happel, J. Viscous flow relative to arrays of cylinders. *AIChE J.* **1959**, *5*, 174–177. [[CrossRef](#)]
176. Lock, S.S.M.; Lau, K.K.; Ahmad, F.; Shariff, A.M. Modeling, simulation and economic analysis of CO₂ capture from natural gas using cocurrent, countercurrent and radial crossflow hollow fiber membrane. *Int. J. Greenh. Gas Control* **2015**, *36*, 114–134. [[CrossRef](#)]